6-1-1979

Design Considerations in Linear Microdensitometry

Thomas Lianza

DESIGN CONSIDERATIONS IN LINEAR MICRODENSITOMETRY

by

Thomas A. Lianza

A thesis submitted in partial fulfillment of the requirements for the degree of Master of Science in the School of Photographic Arts and Sciences in the College of Graphic Arts and Photography of the Rochester Institute of Technology.

June, 1979

Signature of the Author Thomas A. Lianza

Photographic Science and Instrumentation

Certified by Mohamed Abouelata

Thesis Advisor

Accepted by John F. Carson

Coordinator, Graduate Program

School of Photographic Arts and Sciences
Rochester Institute of Technology
Rochester, New York

CERTIFICATE OF APPROVAL

MASTER'S THESIS

This is to certify that the Master's Thesis of Thomas A. Lianza has been examined and approved by the thesis committee as satisfactory for the thesis requirement for the Master of Science degree

Professor Mohamed Abouelata

Professor John F. Carson

Professor Gerhard W. Schumann

2/19/79
Date

DESIGN CONSIDERATIONS IN

LINEAR MICRODENSITOMETRY

by

Thomas A. Lianza

Submitted to the Photographic Science and Instrumentation Division in partial fulfillment of the requirements for the Master of Science degree at the Rochester Institute of Technology

ABSTRACT

The conditions for linearity in microdensitometry are discussed. It is shown that under proper conditions a microdensitometer may behave linearly regardless of the coherence properties of the source.

A linear microdensitometer was constructed and design considerations are presented as well as test results.

ACKNOWLEDGMENTS

This work was funded, to a great extent, by the C.I.A. I am grateful to that organization for their aid and encouragement. Dick Swing was a great help. He taught me the necessary approaches to solve the problem and our conversations were always a great delight. I would also like to thank all those in the department who helped me along in this endeavor: Professor Schuman, Professor Carson, and my advisor Professor Abouelata.

TABLE OF CONTENTS

TABLE OF FIGURES

LIST OF TABLES

1. Introduction

The instrument described in this work is a realization of a theory brought to light by D. Grimes[1]. It is not the first "linear" microdensitometer ever built[2,3,4], but it does differ in certain areas such as choice of light source, drive and control functions. The optics of such instruments are basically constrained by the physics of the operation and there is little deviation from commercially available instrumentation[4].

The difference between the "classical" microdensitometer and the "linear" are not great. The classical microdensitometer can be made to operate in a linear fashion[5] if restraints are placed upon the highest sample frequency that is to be measured. The general optical scheme of both style machines is presented in figure 1.

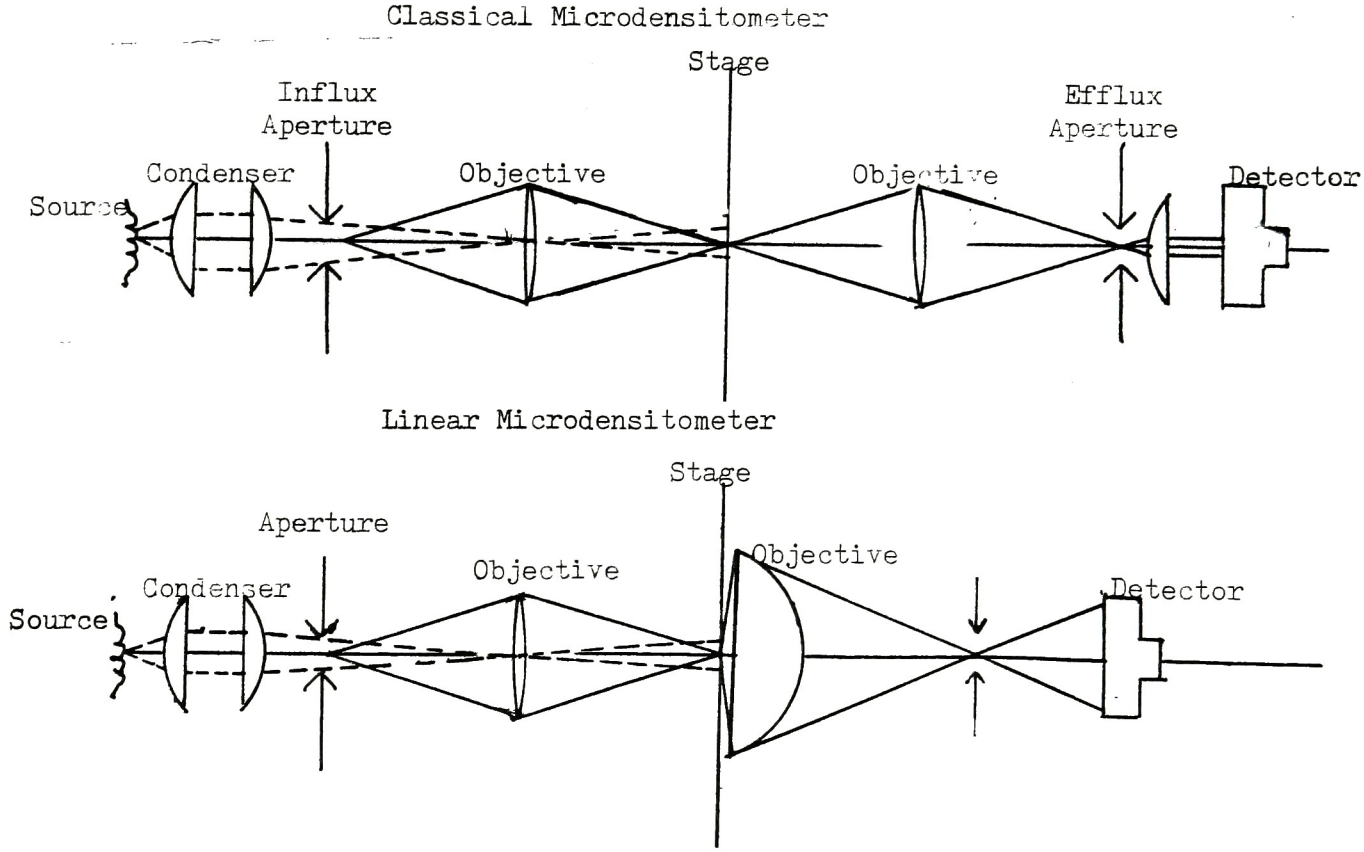

Figure 1 Comparison of Linear and Classical Optics

From figure 1 it can be seen that both systems are identical until the sample is encountered. In the classical machine the sample is re-imaged onto a screen aperture in the same way that a slide is imaged onto a screen by a slide projector. The flux collected by the efflux optics and the efflux aperture is measured and converted to the required information via electronic systems. The optical considerations of this configuration have been discussed to great length [3,4] and will be treated in a less rigourous fashion in the following section of this report.

The linear microdensitometer projects a reduced image of the influx aperture onto the sample plane. The flux transmitted by (not the image of) the sample is collected and measured. One can see that the entire efflux microscope system of the classical machine has been replaced by a condenser which is used to collect all the transmitted flux. The transmitted flux is then electronically measured, converted to optical density, and recorded.

The classical microdensitometer measures semi-specular density while the linear version measures the more commonly used diffuse density. One would then expect that it would be easier to correlate macro/micro density for conversion and comparison. It should also be noted that the classical version relies upon two focusing systems. As the influx system changes focus so does the general level of illumination. This has grave effects upon the photometric integrity of the entire system. In the linear machine, as small excursions from proper focus occur, there is no change in general level because of the collection properties of the efflux collector. The effect of influx defocus of the linear machine is to

generally lower the spatial frequency response of the machine. Defocus of either efflux or influx systems of the classical instrument will degrade photometric performance with the added disadvantage of degraded spatial frequency response in the case of efflux defocus.

It is obvious that the linear design does offer some advantages over the classical design in terms of analysis and ease of construction and it is for these purposes that this project was performed. Other considerations are also important in the design of a microdensitometer and these are considered in greater depth in the Section 3 entitled "Implementation."

The present design is not without problems, but this is to be expected of any prototype system. A careful review and recommended course of correction is presented at the end of this paper as a guide for future work. It is hoped that more work and further calibration will be done on this model and truly unique working system can be developed for research purposes

2. Theory

2.1 A system-operator approach for analysis

No analysis of linear systems would be complete without some excursions into other systems. Three systems and their subsequent analysis will be dealt with in this section: The General System, The Linear System and the Stationary Linear System. In each case, there will be a function, $g(x)$, which is a direct consequence of a system-operator $S\{\ \}$ which alters the input system signal $f(x)$. If the system has some linear response, $h(x)$, the system-operator will apply this response to the input signal.

A general system is depicted in figure 2

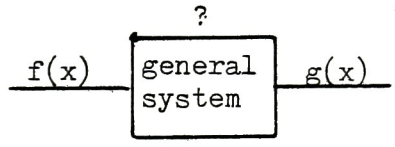

$$g(x) = S\{f(x)\}$$

Figure 2 General System Realization

The response function of this system is unknown, but it does have operational characteristics which alter $f(x)$ such that $g(x) \equiv S\{f(x)\}$. The system response function may be random, or a nonlinear function of x, or any general function. Because the response function is unknown, no information about $f(x)$ can be obtained from $g(x)$. A practical example of such a system would be a correlator. While the output of a correlator is based upon its input signal, the input signal cannot be synthesized from the output signal alone. Such a system cannot be used to estimate input signals, but it could be used to estimate parameters of the input signal.

A linear system, is one whose output is a sum of weighted input components

$$g(x)= S\{af_1(x)+bf_2(x)\ldots\} = aS\{f_1(x)\}+bS\{f_2(x)\} \ \ldots$$

In this sense, the operator is distributive and is then included in the weighting procedure if any. This also implies that the operator is "well behaved" over the region of consideration.

If $f(x)$ is continuous, the sifting property of the Dirac function allows $f(x)$ to be considered one such linear combination of weighted and displaced δ-functions.

1) $$f(x) = \int f(\eta)\,\delta(x-\eta)\,d\eta$$

If $f(x)$ is operated upon by some system, the output, $g(x)$, if given by:

2) $$g(x) = S\{f(x)\} = S\left\{\int f(\eta)\,\delta(x-\eta)\,d\eta\right\}$$

If $f(x)$ is considered a weighting function applied to the δ-functions the operator function may be brought into the integral as a consequence of the definition of linearity given earlier and:

3) $$g(x) = \int f(\eta)\,S\{\delta(x-\eta)\}\,d\eta$$

Letting $h(x\,|_{x=\eta})$ be the response function of the system at the point x due to a δ-function input at η, we have the following:

4) $$h(x\,|_{x=\eta}) \equiv S\{\delta(x-\eta)\}$$

The output may be deduced to be as given in 5):

5) $$g(x) = \int f(\eta)\,h(x\,|_{x=\eta})\,d\eta$$

This is diagrammed in figure 3:

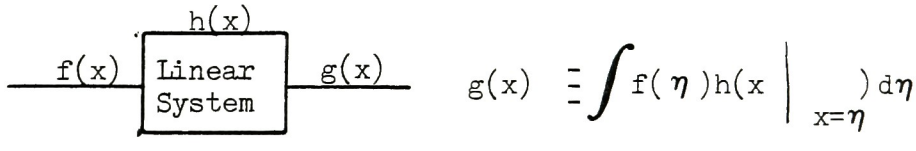

Figure 3 Linear System Realization

In (5), $h(x \mid_{x=\eta})$ may be thought of as the system response function at the point x due to a δ-function at η. In some systems, the response is invariant with position. This would be a stationary system and a further simplification may be made through use of the convolution properties of stationary systems:

$$g(x) = \int f(\eta)h(x-\eta)d\eta \tag{6}$$

This is shown in figure 4

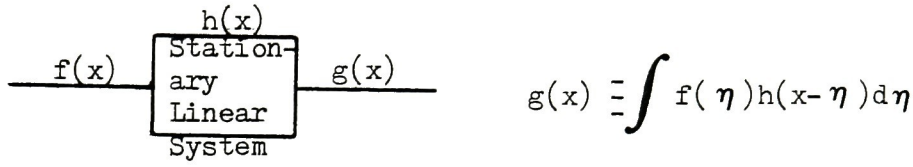

Figure 4 Stationary Linear System

In many electronic systems and their subsequent analysis, the concepts of stationarity and linearity can be assumed. In optical systems the assumption of stationarity is <u>not</u> reasonable over the entire field, but may be assumed over a very small portion of the response surface. This is usually taken to mean the paraxial region in an optical system. In the following discusions stationarity <u>is</u> assumed and all paraxial approximations are made. If these assumptions are not met, the analysis of the problem becomes difficult and non unique.

2.2 Linearity and the Concept of Coherence

In the discussions of stationary linear systems which are used in conjunction with some form of analog detector, it is necessary to consider what the detector is actually detecting.

When discussing these stationary linear systems it is also important to separate the concepts of stationarity and linearity such that stationarity refers to a system's response and linearity concerns the effect that the response has upon an input signal. It will be shown, that depending upon detection considerations, an optical system may or may not be considered linear. It will further be shown that linearity is a direct result of the coherence of a given signal and subsequent detection. The temporal bandwidth of modern detectors is still small when compared to the frequencies encountered in visible radiation (i.e., light). This deficiency will cause any measurement of radiant intensity* to be a time-averaged process. It will be shown that this time-averaging yields different results which are dependent upon temporal qualities of the light source under consideration. The discussion will be based primarily upon correlation considerations. If there is no correlation (time, or space) in an optical field, the signal will be considered incoherent. As the correlation increases, so will the coherence. It will further be shown that coherent optical systems are inherently non-linear upon detection.

Consider the optical system diagrammed in Figure 5.

---

* The term "intensity" should not be interpreted in the normal radiometric sense: Power per unit solid angle. For the purposes of the following discussion intensity will be a time averaged quantity which is more closely related to irradiance in definition, but because it relates to individual points in a field rather than some unit of area of the field, distinction is made.

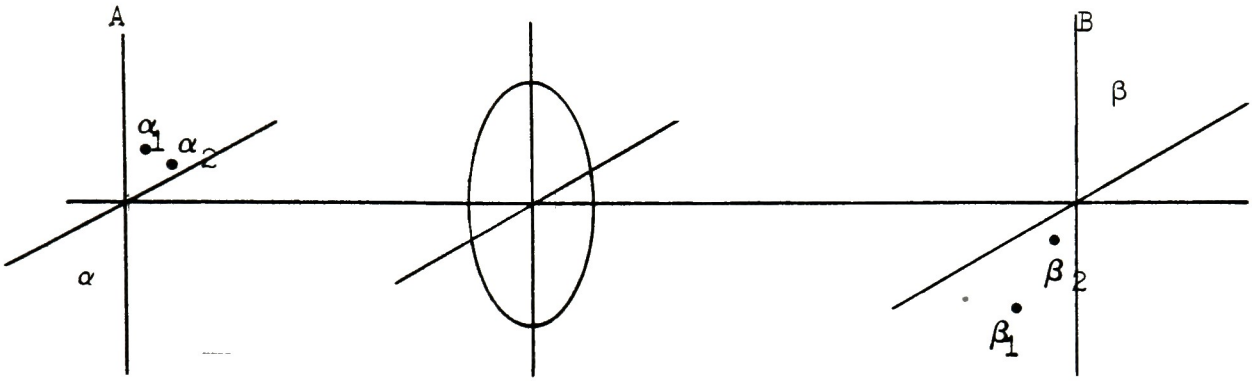

Figure 5 General Optical Model

It will be assumed that the lens has an irradiance impulse response given by $S(\beta) \equiv K(\beta)K^*(\beta) \equiv |K(\beta)|^2$ where $K(\beta)$ is the amplitude response of the lens. An optical field $\psi_{object}(\alpha, \tau)$ is imaged onto the B plane to produce an image field $\psi_{image(\beta,\tau)}$ such that

7) $$\psi_{image}(\beta, \tau) = \int \psi_{object}(\alpha, \tau) K(\beta - \alpha) d\alpha$$

$\psi_{image(\beta,\tau)}$ is not observable because of the temporal bandwidth of the detector and is then recorded as a time-averaged function $\epsilon_{image(\beta)}$ such that

8) $$\epsilon_{image}(\beta) \doteq \underset{\beta_1 \to \beta_2 \to \beta}{<\psi_{image}(\beta_1, \tau)\, \psi^*(\beta_2, \tau)>}$$

Where $< >$ denotes the time average. The average in general of $f(\tau)$

$$9) \qquad <f(\tau)> = \lim_{\tau \to \infty} 1/2T \int_{-T/2}^{+T/2} f(\tau)\, d\tau$$

From 7 it may be shown that:

$$10) \qquad \epsilon_{image}(\beta) = <\int \psi_{object}(\alpha, \tau) K(\beta - \alpha)\, d\alpha \int \psi^*_{object}(\alpha', \tau) K^*(\beta - \alpha')\, d\alpha >$$

$$11) \qquad \epsilon_{image}(\beta) = \iint <\psi_{object}(\alpha, \tau)\, \psi^*_{object}(\alpha', \tau)> K(\beta - \alpha) K^*(\beta - \alpha')\, d\alpha\, d\alpha'$$

Equation (11) is general in as much as no coherence bounds have been placed upon it, and the assumption is made that the spectral bandwidth considered is small when compared with the total bandwidth i.e. quasi-monochromatic assumption is inferred.

In totally incoherent illumination, light from each point in the object plane is assumed to be statistically independent of the light from all other points. Under this condition (ideally):

$$12) \qquad <\psi_{object}(\alpha, \tau)\, \psi^*_{object}(\alpha', \tau)> = \epsilon_{object}(\alpha)\, \delta(\alpha, \alpha')$$

Substitution of (12) into (11) yields:

13) $$\epsilon_{image}(\beta) = \iint \epsilon_{object}(\alpha)\,\delta(\alpha - \alpha')K(\beta - \alpha)K^*(\beta - \alpha')\,d\alpha\,d\alpha'$$

Integration over α' yields:

14) $$\epsilon_{image}(\beta) = \int \epsilon_{object}(\alpha)K(\beta - \alpha)K^*(\beta - \alpha)\,d\alpha$$

But:

15) $$S(\alpha) = K(\alpha)K^*(\alpha) = \left|K(\alpha)\right|^2$$

and it may then be said that:

16) $$S(\beta - \alpha) = K(\beta - \alpha)K^*(\beta - \alpha)$$

Therefore:

17) $$\epsilon_{image}(\beta) = \int \epsilon_{object}(\alpha)S(\beta - \alpha)\,d\alpha$$

which is characteristic of a linear stationary system as defined in Equation (6).

In coherent illumination, the light at any one point in the plane under consideration is correlated with all points and it may be described by what is termed the mutual intensity function. Refering to Figure 5 one sees the points (α_1,α_2) and (β_1,β_2) in the A and B planes respectively. The mutual intensity function will describe the complex degree of coherence about these two points and is given as:

18) $$\Gamma_{12}(\tau) = \Gamma(\alpha_1, \alpha_2, t) = \langle \psi(\alpha_1, \tau)\, \psi^*(\alpha_2, t+\tau) \rangle$$

Because of the high degree of interdependance between points in the field, the time average can no longer be realistically thought of as an intensity function multiplied by a shifted δ-function, but must be realized by a function of the complex amplitude in the field as in (19).

19) $$\Gamma_{12} = \langle \psi_{object}(\alpha_1)\ \psi^*_{object}(\alpha_2) \rangle$$

Substitution into (11) yields

20) $$\epsilon_{image}(\beta) = \iint \psi_{object}(\alpha_1)\, \psi^*_{object}(\alpha_2) K(\beta - \alpha_1) K^*(\beta - \alpha_2)\, d\alpha_1\, d\alpha_2$$

and integrating over α_2 as in (14)

21) $$\epsilon_{image}(\beta) = \left\langle \left| \int \psi_{object}(\alpha_1) K(\beta - \alpha_1)\ d\alpha_1 \right|^2 \right\rangle$$

The complex amplitude associated with the object field is convolved with the amplitude function of the system. The modulus squared of this result is a consequence of the detector qualities. It should be noted that coherent systems are linear in complex amplitude, but detected in a time averaged mode which is incapable of measuring the complex amplitude variations. A partially coherent system may be described by a mutual intensity function and this will also be linear until detection.

2.3 Imaging in the Classical Microdensitometer

A completely rigorous approach to the imaging problem in the classical microdensitometer is beyond the scope of this work, but for the purposes of comparison, it is necessary to consider the classical system in some degree of depth.

The problem of propagating light through an optical system is not straight forward unless one realizes some essential facts as well as the approach.

The approach will be as follows: (see reference (2,3))

1. Characterize the light at the illuminating plane by a generalized mutual intensity function: $\Gamma(\alpha_1,\alpha_2)$. This function acts as a general descriptor of the coherent properties of the source in question. It is a correlation function. High correlation indicates coherence, little or no correlation indicates incoherence.

2. Assuming paraxial optics, two "propagators" arise. (See Appendix 1.)

$$\exp(ik(p_1 - q_1)^2/2s)\exp(-ik(p_2-q_2)^2/2s$$

i is the square root of -1, p represents a coordinate in the starting plane, q is the coordinate in the plane to which the wave is headed. $k = 2\pi/\lambda$. s is the distance of propagation. Note that the mutual intensity function was characterized by two points; as a result, both points must be propagated through the system.

3. A lens in the optical system adds another term: (See Appendix 2.)

$$F(p_1)F^*(p_2)\exp(ik(p_2^2 + p_1^2)\ /2f$$

This accounts for the lens pupil function and the convergence of a plane wave resulting from a lens.

4. Using 2 & 3, we then will continue propagating this mutual intensity function through the system. After simplifying the expression as much as possible by assuming the sample to be in focus and factoring, specific situations will be applied to the end result and the flux reaching the sensor aperture will be identified.

5. The end result will yield a function of the source aperture mutual intensity function, the shifted sample, the sensor function, and two Fourier kernals representing the transform of the pupil function of each lens.

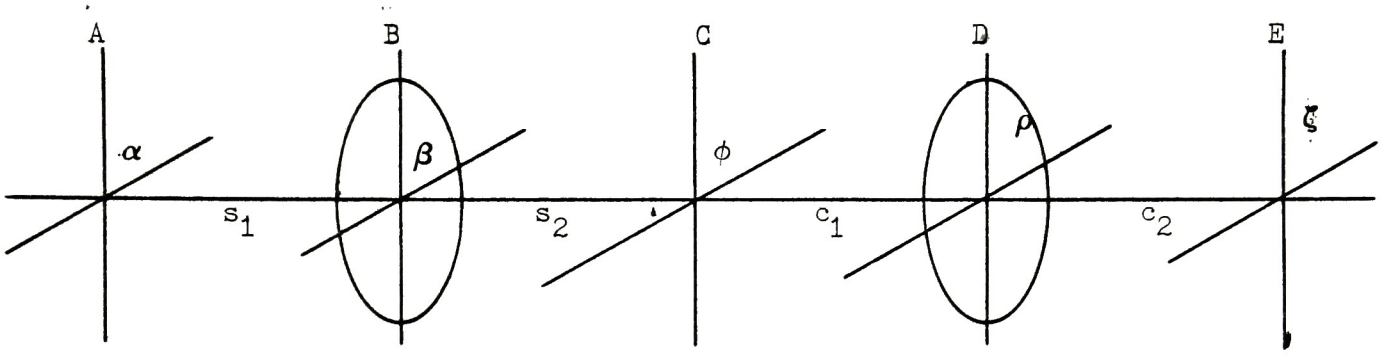

Figure 6 General Microdensitometer Model

The light will be propagated from the source aperture towards the sensor aperture. Plane A represents the source aperture as labeled and plane E is the collector aperture. Starting at the source aperture we find:

$$22)\quad \Gamma(\beta_1, \beta_2) = \int \Gamma_o(\alpha_1, \alpha_2) A(\alpha_1) A^*(\alpha_2) \exp(ik(\beta_1 - \alpha_1)^2/2s \times \exp(ik(\beta_2 - \alpha_2)^2/2s_2) d\alpha_1 d\alpha_2$$

Now propagate this result through the lens at B:

$$23)\quad \Gamma(\phi_1, \phi_2) = \int \Gamma(\beta_1, \beta_2) B(\beta_1) B^*(\beta_2) \exp\left[-ik(\beta_1^2 + \beta_2^2)/2f\right] \times \exp\left[ik(\phi_1 - \beta_1)^2/2s_2\right] \exp\left[-ik(\phi_2 - \beta_2)^2/2s_2\right] d\beta_1 d\beta_2$$

At plane C it is necessary to introduce a shift of η because the sample is in motion.

$$24)\quad \Gamma(\rho_1, \rho_2, \eta) = \int \Gamma(\phi_1, \phi_2) C(\phi_1 - \eta) C^*(\phi_2 - \eta) \exp\left[ik(\rho_1 - \phi_2)^2/2c_1\right] \times \exp\left[-ik(\rho_2 - \phi_2)^2/2c_1\right] d\phi_1 d\phi_2$$

When the light has been attenuated by the sample, it is collected by the efflux lens:

$$25)\quad \Gamma(\zeta_1, \zeta_2, \eta) = \int \Gamma(\rho_1, \rho_2, \eta) D(\rho_1) D^*(\rho_2) \exp\left[-ik(\rho_1^2 + \rho_2^2)/2f\right] \times \exp\left[ik(\zeta_1 - \rho_1)^2/2c\right] \exp\left[-ik(\zeta_2 - p_2)^2/2c_2\right] \times E(\zeta_1) E^*(\zeta_2) d\rho_1 d\rho_2$$

This final integration describes the mutual intensity function at the efflux (sensor, collecting) aperture. Photomultiplier tubes do not measure mutual intensity, but they do measure flux. The limit of this mutual intensity function must be found as ζ_1 converges to $\zeta_2 = \zeta$ so that:

$$26)\quad P(\zeta, \eta) = \lim_{\zeta_1 \to \zeta \leftarrow \zeta_2} \Gamma(\zeta_1, \zeta_2, \eta)$$

The flux collected by the sensor as a function of the shift is given by integrating equation (25):

$$27)\quad P(\eta) = \int P(\zeta, \eta) d\zeta$$

In equation (25) the last two terms describe the complex transmissive characteristics of the sensor aperture.

28) $$E(\zeta_1)E^*(\zeta_2) = F(\zeta)$$

In reference 6, Swing goes through the mechanics of simplifing equation (25) into an understandable form, based on physical reasoning. It is <u>not</u> straightforward unless the microdensitometer is in good focus. This operation leaves a function which is shifted, contains the sensor function, the source aperture mutual intensity function, and the two Fourier kernals representing the Fourier transform of the pupil function of each lens.

29) $$\phi(\eta) = \int \Gamma(\alpha_1, \alpha_2)C(\phi_1 - \eta)C^*(\phi_2 - \eta)F(\zeta) \quad x$$

$$\widetilde{B}(\alpha_1/\lambda s_1 + \phi_1/\lambda s_1)\widetilde{B}^*(\alpha_2/\lambda s_2 + \phi_2/\lambda s_2) \quad x$$

$$\widetilde{D}(\phi_1/\lambda c_2 + \eta/\lambda c_2)\widetilde{D}^*(\phi_2/\lambda c_2 + \eta/\lambda c_2)$$

$$d\alpha_1 d\alpha_2 d\phi_1 d\phi_2 d\zeta$$

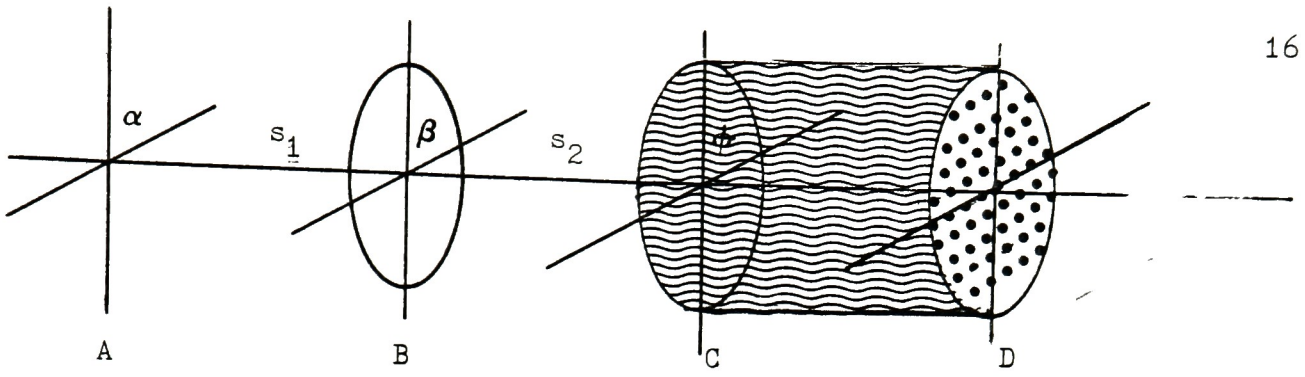

Figure 7 Linear Microdensitometer Model

2.4 The Linear Microdensitometer

The analysis of the linear configuration as depicted in Figure 7 should be straightforward in light of the previous discussion of the classical microdensitometer. The influx optics are described as in Equations (22 - 24). Neglecting the shift in the sample, for the moment, intensity at plane "C" is given by:

$$30)\ \epsilon = \int \Gamma(\alpha_1\alpha_2)A(\alpha_1)A^*(\alpha_2)\exp(ik(\beta_1 - \alpha_1)^2/2s_1) \quad x$$

$$\exp(-ik(\beta_2 - \alpha_2/2s_1)B(\beta_1)B^*(\beta_2)\exp(-ik(\beta_1^2 + \beta_2^2)/2f_{influx} \quad x$$

$$\exp(ik(\phi_1 - \beta_1)^2/2s_2)\exp(-ik(\phi_2 - \beta_2)^2/2s_2$$

$$C(\phi_1)C^*(\phi_2)d\alpha_1 d\alpha_2 d\beta_1 d\beta_2 d\phi_1 d\phi_2$$

The term $C(\phi_1)C^*(\phi_2)$ specifies the complex amplitude transmissive characteristics of the sample. Once again the measureable quantity is the power transmission characteristic of the sample and we have:

$$31)\qquad t(\phi) = |C(\phi)|^2 = C(\phi_1)C^*(\phi_2)$$
$$\phi_1 \to \phi_2 \to \phi$$

Assuming that the influx aperture is imaged infocus upon the sample in the plane "C", and the paraxial assumptions are valid, it can be shown that the irradiance measured through the plane is of the form:

32) $$\epsilon = \int t(\phi)h(\bar{\phi})d\bar{\phi}$$

where 33) $$h(\phi) = \int \Gamma(\alpha_1, \alpha_2)A(\alpha_1)A^*(\alpha_2)B(\beta_1)B^*(\beta_2)$$

$$\exp(ik(\beta_2\alpha_2 - \beta_1\alpha_1)/s_1)\exp(-ik\,\phi\,(\beta_2 - \beta_1)/s_2$$

$$d\alpha_1 d\alpha_2 d\beta_1 d\beta_2$$

Assuming that the sample is now shifted by an amount "x", the output becomes:

34) $$\epsilon(x) = \int t(x - \phi)h(\phi)d\phi$$

Which is essentially a linear system with a δ-function response of $h(\phi)$.* Furthermore, if the aperture is imaged in such a fashion that it is no longer resolved,* Equation (33) may be written as:

35) $$h(\phi) = \left| \int B(\beta)\exp(ik\,\phi\beta/s_2)d\beta \right|^2$$

The consequence of (35) is that the coherence at the source slit is no longer a consideration in the imaging process. This would allow one to use any source, coherent or otherwise. This flexibility along with the

---

* let $A(\alpha_1)A^*(\alpha_2) = \delta(\alpha)$

need to focus only one side of the optical system is very attractive from the standpoint of ease of construction. It is assumed that all of the flux is collected past plane "C" and that this is measured by the photo-detector. If the situation depicted in Equations (34) and (35) are valid, then this instrument is indeed linear and is of the form of Equqtion (32). Conspicuously missing from the literature[1,2,3,4,5,6] is the problem associated with large apertures (i.e., resolvable apertures) and sample scattering. Effectively, the "modulus-squared" of the input function is taken only upon collection and subsequent detection of the signal. In the actual operational situation a piece of relatively noisy photo-graphic film would be in the sample plane. Regardless of the efficiency of the collector the scattering introduced by illumination by a large, coherent aperture will be dependent upon the sample's frequency content. This is not constant with density nor is it constant from sample to sample The problem of scatter has been treated in certain studies[3,4], but this was assuming that an unresolved aperture was imaged onto the image plane. The only way to combat the problem of scatter with larger apertures is to put a very large detector in contact with the sample plane. The present day practice is to use a high numerical aperture condensor, which by its very nature is limited to an efficiency of 84%[6].

3. Implementation

This section describes the approach and implementation to each sub-assembly of the microdensitometer. Any theory or fundamental idea specific to the particular sub-assembly and not general to linear microdensitometry is found in this section.

3.1 The Stage

3.1.1 General Description

A microdensitometer would be of no value if it could not measure spatial variations in a sample by accurately scanning the sample. For measurements involving linear analysis it is essential that spatial integrity be maintained. It is also important that equidistant samples be taken for analysis involving Fast Fourier Transform algorithms (FFT's).

Since a new stage could not feasibly be budgeted, it was decided to use the stage of an Ansco Model IV microdensitometer. Because it is back sprung, the stage is constantly under stress from one direction. It is driven by a metric micrometer (1 rev./.500 mm) and is capable of travel of about 1 cm. from center in either direction. This is really not restrictive when considering the maximum number of points that could be collected is on the order of 10,000. The short scanning distance also allows for other advantages:

1. It is driven by a micrometer thread which is of generally higher quality and lower cost than commercially available lead screws.
2. It is easier to align the stage for good focus over the entire scanning range.
3. The backspring eliminates inertial forces and lessens stage "jitter".

3.1.2 Sampling "on the fly"

Whenever a spatial measurement is made in microdensitometry, it is intrinsically a temporal one also. Consider the Ansco Model IV microdensitometer: the stage is driven at a relatively constant velocity and the signal is recorded on a moving chart recorder. The translation from velocity to spatial increment is a division operation of chart velocity and stage velocity to yield: x inches of chart = y micrometers of displacement on the sample.

If one assumes constant linear stage velocity and that sampling in time is performed, the following may be postulated: We wish to transform some function f(x) (assume a line object used in transfer function analysis) where $x = z_o + vt$ where v is the stage velocity and t a time that a sample is taken, z_o is an initial position. Taking the Fourier transform of f(x) we get:

36) $$\mathcal{F}\{f(x)\} = \int f(z + vt)\exp(-i\omega z)dz = G(\omega)$$

By the shifting property of the Fourier Transform it is shown that:

37) $$G(\omega) = F(\omega)\exp(i\omega vt)$$

The sample is really taken over some finite time interval, T, and it may be shown that when (37) is integrated over the interval -T/2, T/2

38) $$\mathcal{F}\{f(x)\} = F(\omega)T\ \mathrm{sinc}(\omega vT/2)$$

In the case of the Ansco Model IV and similar analog machines that use a stage and a chart recorder, there are two time dependent steps and (38) becomes

39) $$\mathcal{F}\{f(x)\} = F(\omega) T_1 T_2 \operatorname{sinc}(\omega v T_1/2) \operatorname{sinc}(\omega v T_2/2)$$

The effect of (39) can have rather disasterous effects if velocities are high or if point aquisition times are long. In general this is not the case, but the effect manifests itself at higher frequencies.

3.1.3 Drive System Description

To eliminate the problem of sampling on the fly, it was necessary to investigate other methods of drive. Most digital systems use tachometer drives which allow for constant velocity measurement and correction and also accurate sampling. The price of such a system was prohibitive (i.e. greater than $5,000) and it was necessary to find a system that would not need a computer for control or commands. The only system that would accomplish this was the stepping motor system. The stage moves an incremental distance, comes to a rest, a sample is taken, and the process repeated. This would do the job, but there were many considerations to be investigated.

The stepping motor must develop a very high initial torque because it cannot accelerate over a long period of time. Once it gets moving, it cannot rely upon inertia to keep it going or it won't be able to stop. It is then left to the designer of a system incorporating these devices to be certain that the system requires low starting torque and does not develop a lot of inertia during travel. The stage that was available was well suited to the task. Because it was micrometer driven, it required a minimum amount of torque to drive it. The action

of the back spring helped to damp the forward overshoot which would develop the inertia. The stepping motor was judged as a suitable inexpensive means of driving the stage.

At the time of this study, only one system was found to meet the cost/performance requirement: Superior Electric Slo-Syn Stepping Motor Model No. M091-FD06 and a STM1800V control board. The motor characteristics are given in Figure 8.[8]

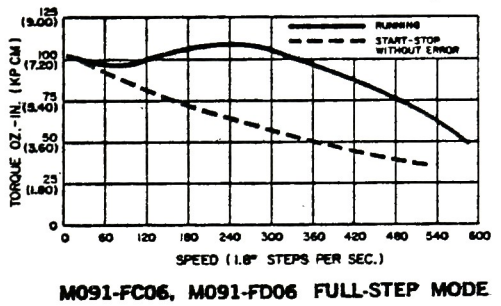

Figure 8 Stepping Motor Characteristics

Slo-Syn motors operate on phase switched DC power[8]. The motor shaft advances 200 steps per revolution when using the STM1800V board. In the current drive system a 200 step sequence is geared 2:1 via a timing belt assembly to yield a 0.9° shaft deflection with a nominal 1.25 micrometer translation. The timing for continuous motion is done by an "on card" oscillator in the control module for the stepping motor.

3.3.4 Digital Control and "pseudo" Spatial Sampling

The digital control of a stepping motor may once again involve sampling "on the fly" if one is not careful about the timing sequence for the sample function.

Consider the motion of an ideal stepping motor operation at low frequency periods to be similar to a Dirac comb (in both time and space) that is use to sample some time invariant but spatially variant function $f(x)$. This is shown in Figure 9.

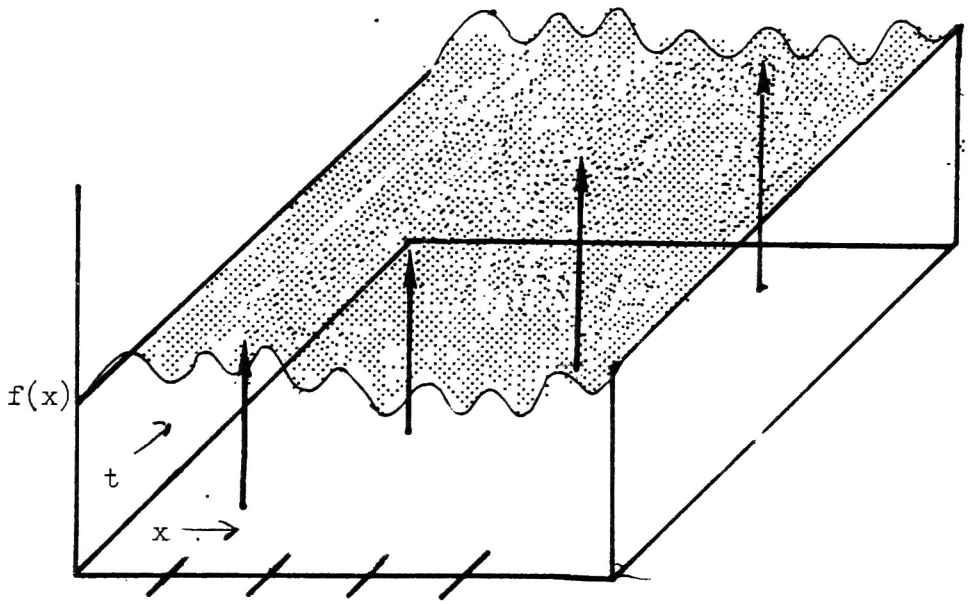

Figure 9 Time-Space Sampling of Temporally Invarient Function

So long as there is no oscillation in time, we are sampling in space and error is only due to position.

Introduction of oscillation in time would be analogous to convolving (in the time dimension) some "jiggle" function, $j(t)$. A diagram of such a system is presented in Figure 10 .

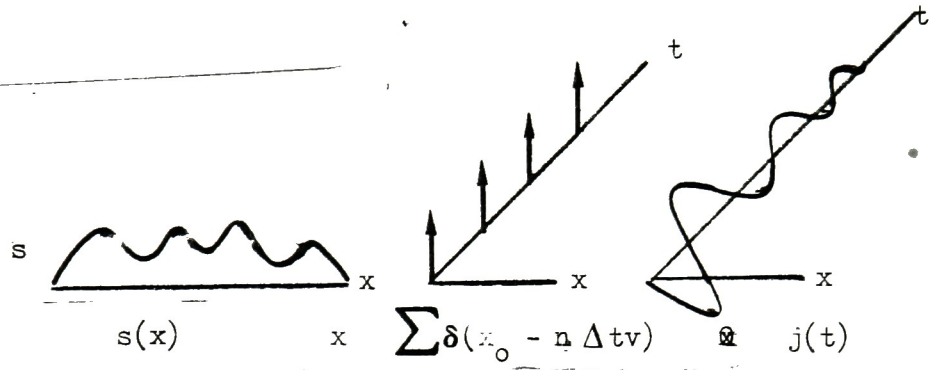

Figure 10 Sampling in Non-Stationary Temporal Space

Looking down on the x, t plane as in Figure 11, the result of $\delta(x - n\,\Delta x) \circledast j(t)$ would appear as in Figure 11

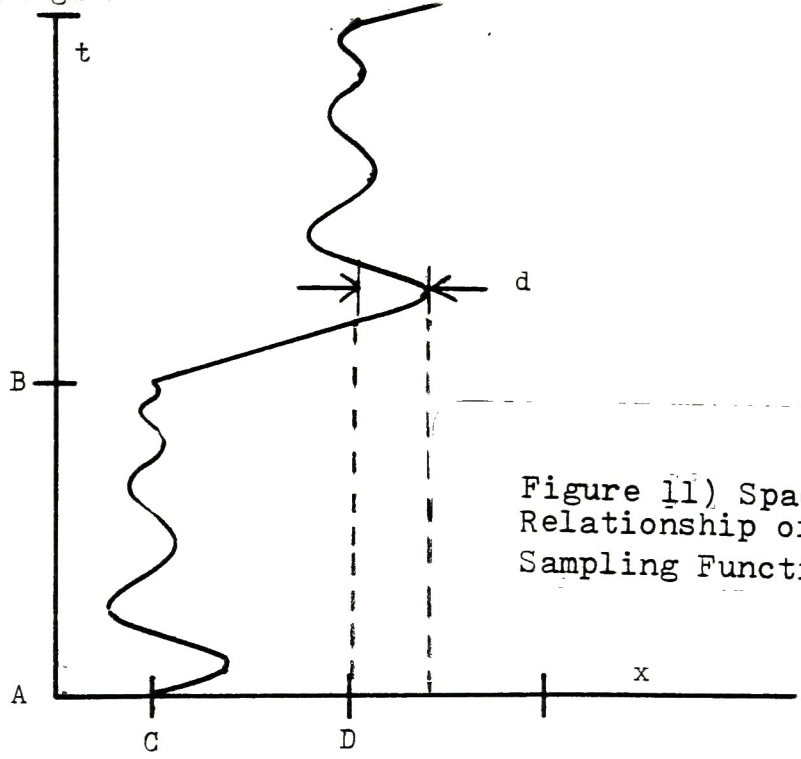

Figure 11) Space-time Relationship of Convolved Sampling Function

The distance AB = period of pulse, CD may be considered the distance travelled . d/CD is the fraction overshoot of the system. The "jiggle"

might be modeled by an exponentially damped sinc function which would be parametrically fitted, but this would provide little information for a general system. Before any digitizing scheme is applied to this system, the period of oscillation must be measured. Figure 12 is a photograph showing the stepping motor and timing belt drive system.

The Scan Mode switch makes provision for single step, or continued stepping. The Chart Constant control controls the speed of scan. The speeds are uncalibrated but may be calibrated by adjusting the trimpots on the board nearest the illuminating subassembly (see Figure 13). The direction control is used to control stage direction.

3.2 Light Source and Spectral Sensitivity

3.2.1 The Light Source

The light source of the microdensitometer was chosen on the basis of cost, reliability, and ease of maintenance. The total collection system and subsequent detection process relaxes, to some degree, the coherence restrictions place upon the sampling aperture so that coherence was not considered a real factor.

A tungsten halogen FDS lamp was chosen as the light source (Figure 14). It exhibits long life (greater than 100 hours) and has a large area filament. The tungsten spectral energy distribution has been well defined and measured. The lamp is powered by 24 volts D.C. so that there is a minimum of A.C. noise

Because Tungsten is essentially a broad band source (as compared to a laser), it may be assumed that the polychromatic transfer function of an optical system that is being illuminated by

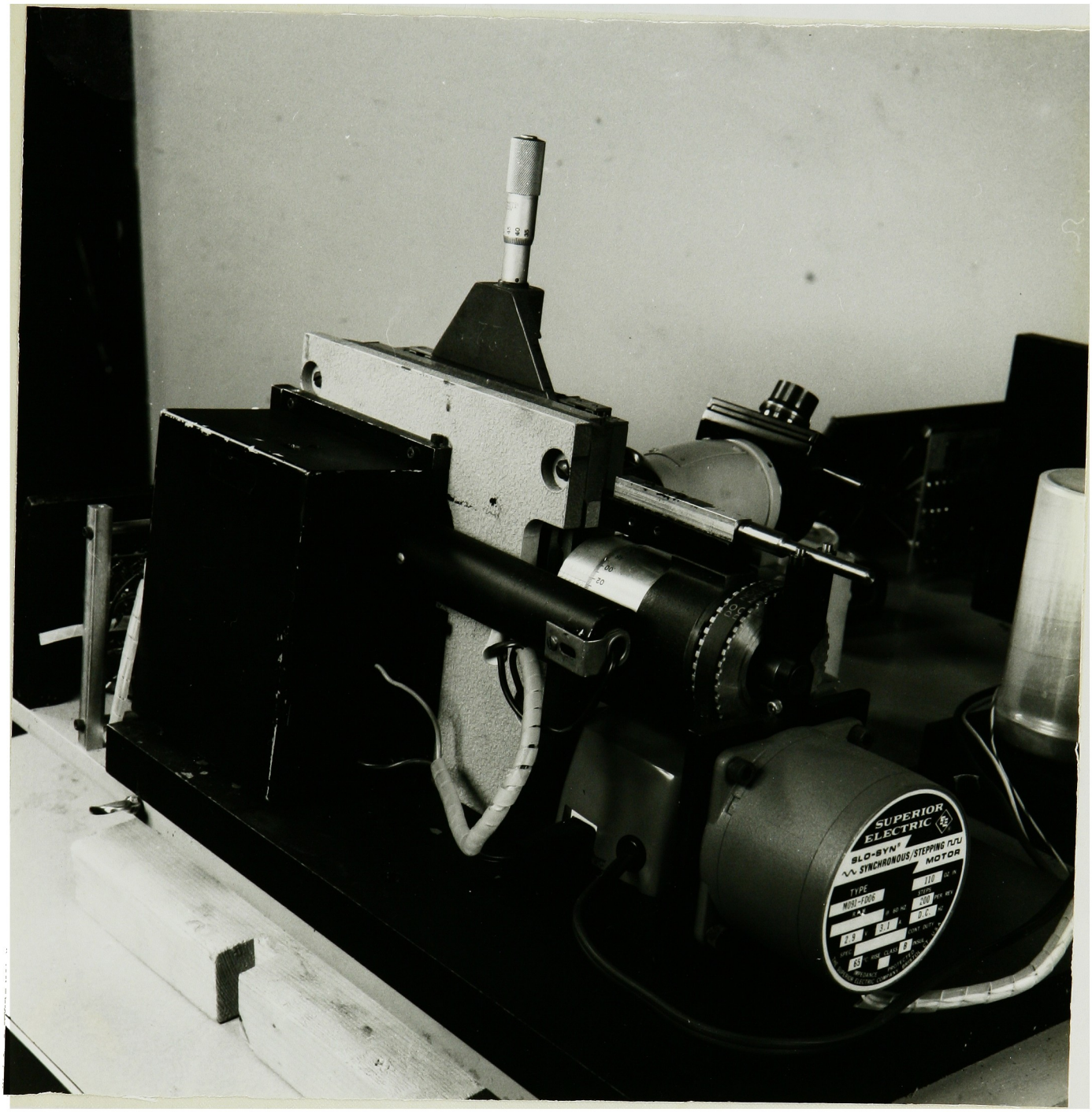

Figure 12. Stepping Motor Drive

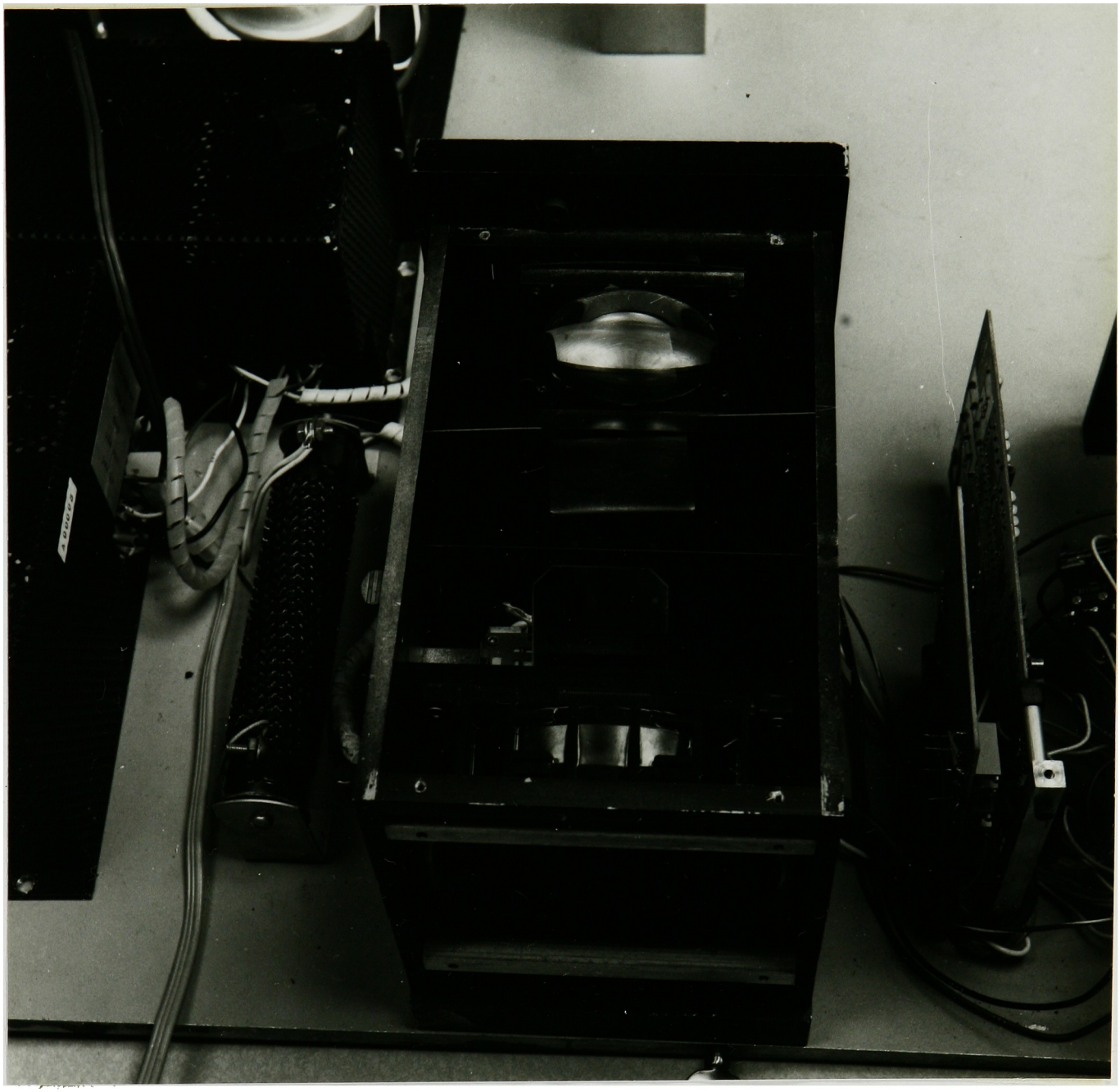

Figure 13. View of Illumination System Showing Timing Trimpots

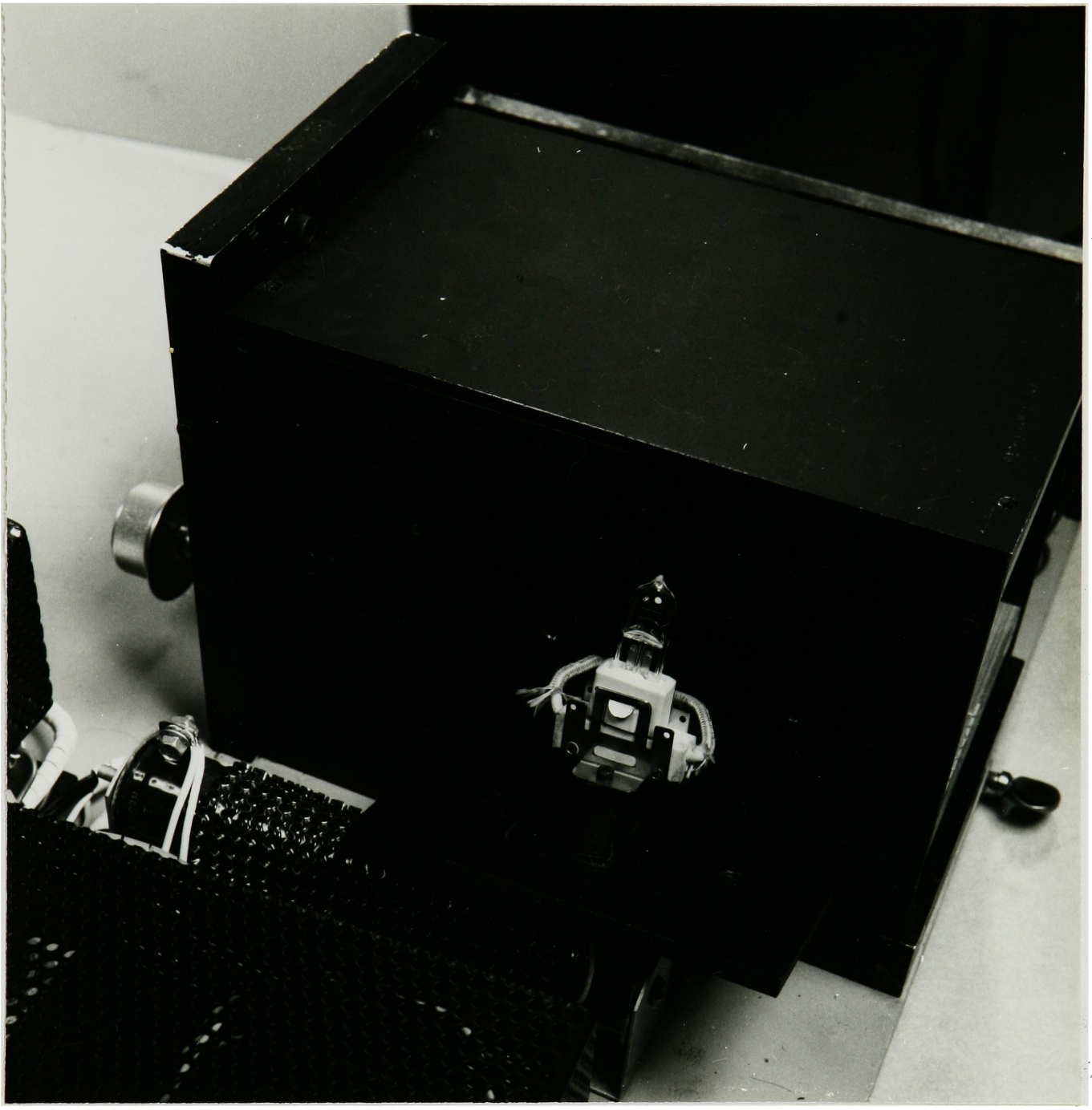

Figure 14. Microdensitometer Light Source

tungsten is essentially a weighted average of all the monochromatic transfer functions over the total bandwidth of detection. The weights are derived from the relative spectral energy distribution. See Figure 15.

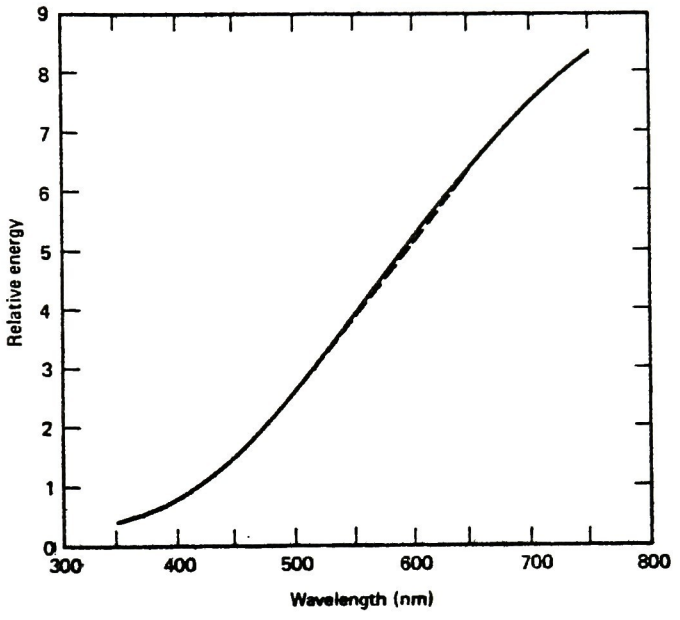

Figure 15 Relative Spectral Energy Distribution of Tungsten Halogen Lamp[7] (at 3000°K)

3.2.2 Spectral Sensitivity Considerations

In addition, the spectral sensitivity of the detector must also be considered. The detector is more fully described in a later section, but its spectral response is plotted in Figure 16.

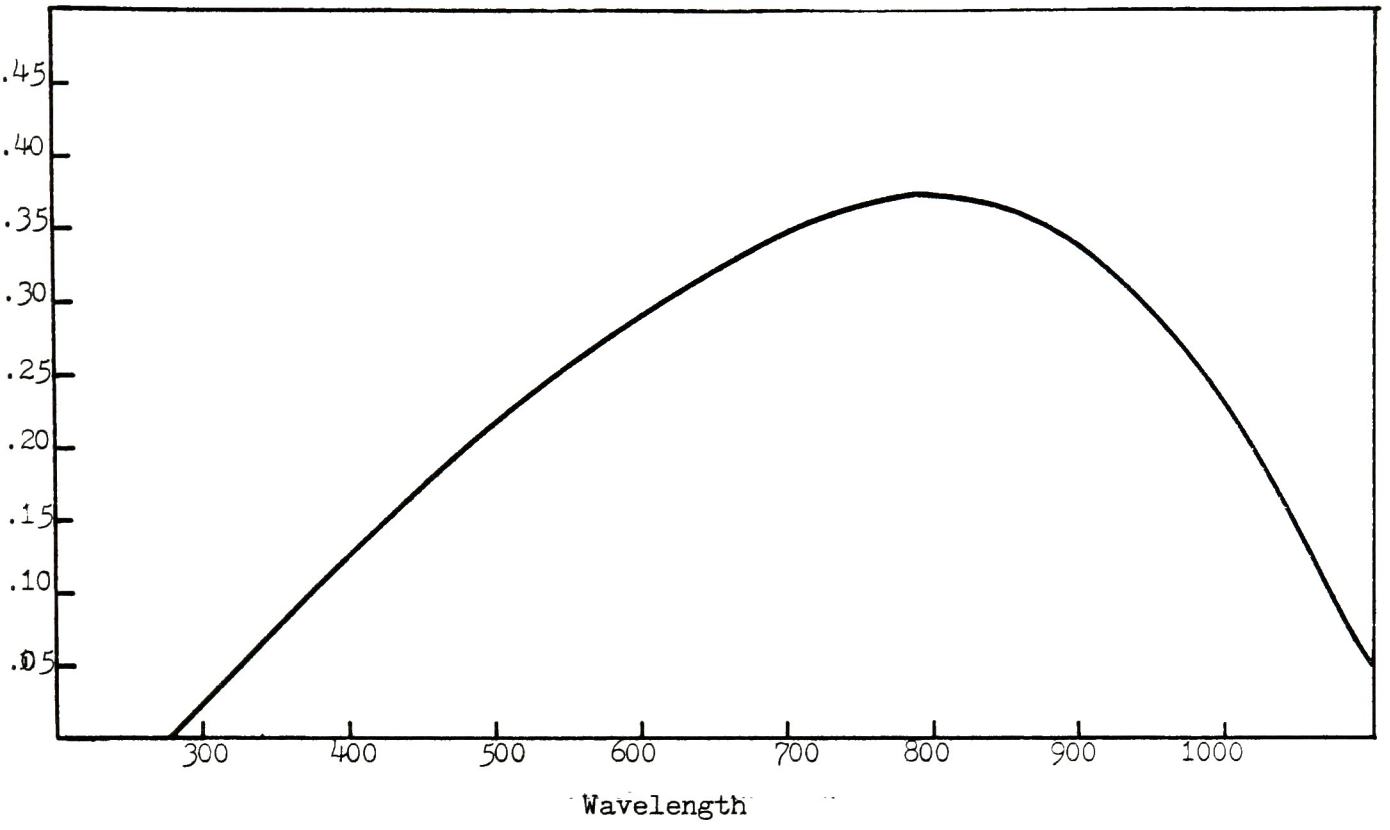

Figure 16 Spectral Response Curve of Photodiode

The diffraction limited OTF of an optical system is given by

$$(1)\quad T(w) = 2/\pi \cos^{-1}\left(\left(w/w_o - w/2w_o\right)\left(1 - (w/w_o)^2\right)^{1/2}\right)$$

$$\text{where } w_o = \frac{2 \times \text{N.A.}}{\lambda} .$$

As λ increases the cutoff frequency of the optical system decreases.

In estimating machine performance, it is therefore necessary to identify what the spectral response of the machine is. It

is noted that both the tungsten and silicon spectral functions extend well beyond the visible red region. Both are seen to peak outside of this region. It is therefore necessary to limit the longer wavelengths passed in order to insure optimum optical response. This necessitated the introduction of a short pass optical filter : Bausch and Lomb 90-660. (See Figure 17)

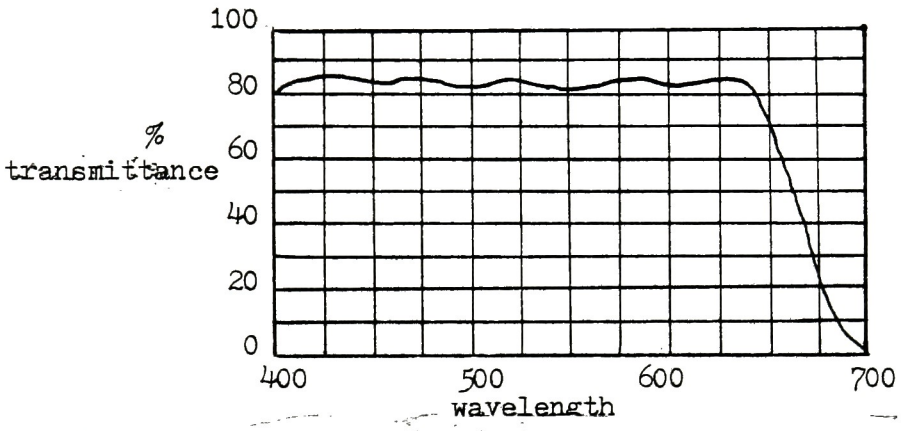

Figure 17 Spectral Transmission of 90-660 filter

The combined relative spectral weighting function is given by cascading the tungsten spectral output, relative silicon response and the filter

transmission such that the spectral response function is given by

$$(2) \quad S(\lambda) = T(\lambda)R(\lambda)F(\lambda)$$

and the normalized

$$S_N(\lambda) = \frac{T(\lambda)R(\lambda)F(\lambda)}{\sum T(\lambda)R(\lambda)F(\lambda)} .$$

This is plotted in Figure 18

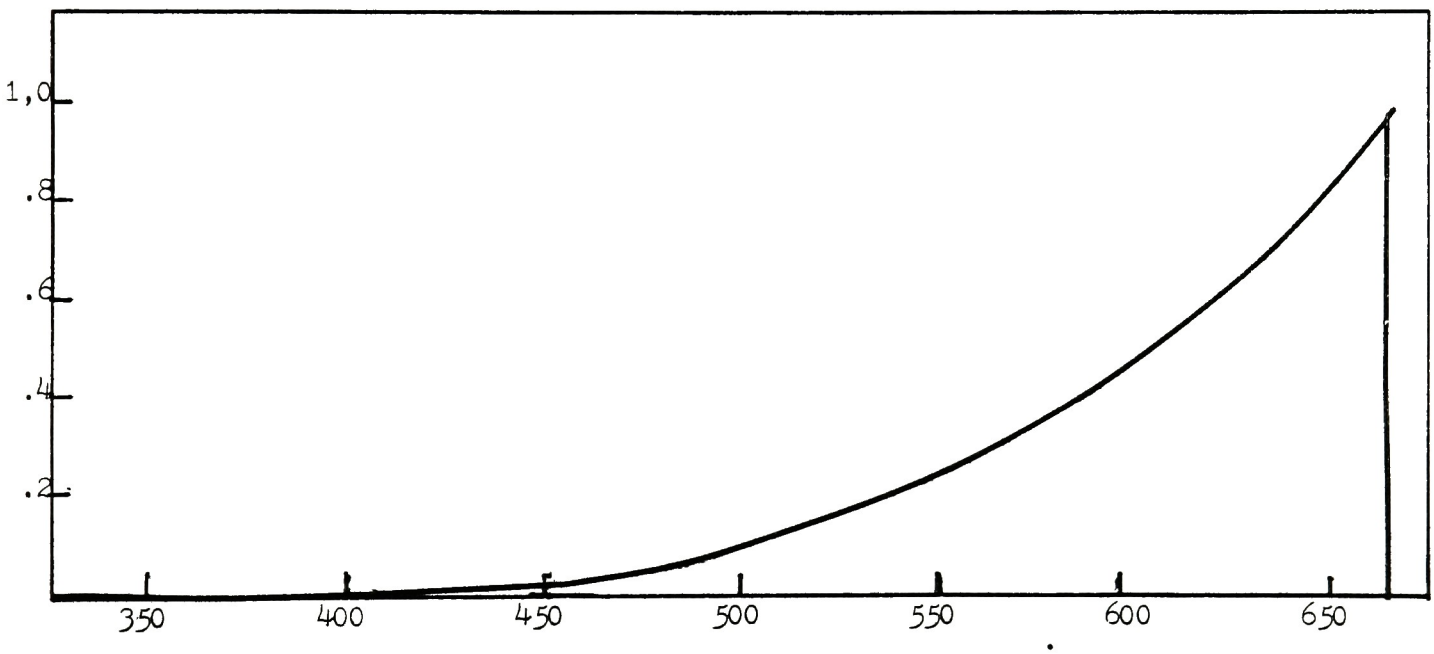

Figure 18 Combined Relative Spectral Weighting Function

From the $S_N(\lambda)$ curve the polychromatic MTF may be calculated in the following manner:

A weighted monochromatic MTF must be calculated for each wavelength and summed over all weights to yield the average polychromatic MTF.

The above calculations should be made with the knowledge that chromatic aberrations have been left out. If the optical system is chromatically aberrated, this technique is not advisable.

3.3 The Receiver and Electronics

In choosing a detector it is necessary to arrive at the proper compromise of features to ensure reasonable operation of the final instrument. These features are:

(1) Sensitivity - Noise Equivalent Power or D* characterizing the lowest energy deviations recorded.

(2) Responsivity - The relative or absolute output as a function of incident wavelength energy.

(3) Speed - step function response

(4) Lifetime Stability - change with time of responsivity

(5) Linearity of Response - number of decades of useable response.

Table 1 compares a number of detectors for the above and other qualities. Of these detectors, three were chosen as possible candidates:

(1) Photoemissive (Photomultiplier tube - PMT)

(2) Photoconductive Schottky-Barrier (Junction)

(3) Photoconductive Diffused (Junction).

It is obvious, that in terms of sensitivity alone, the PMT is clearly the best choice, but there are other factors which enhance

Table 1 **Comparisons of Photosensors** [7]

(Listed in Order of Preference or Capability for Selected Conditions)

	Spectral Response			Threshold Sensitivity	Responsivity	Dark Current	Size and Weight	Long-Time Stability	Power Consumption	Temperature Sensitivity	Sturdiness	Linearity	Power Dissipation	Power Supply Required	Time of Response	Compatability with Integrated Circuits	Maximum Temperature	Bilateral Current	Overload Recovery	Capability	Multielement Flexibility
	UV	VIS	IR																		
Bulk photoconductors																					
CdS	5	1	5	2	3	3	3	4	3	3	1	4	1	Lv[a]	7	6	2	1	5	4	
CdSe	6	3	4	3	3	4	3	4	3	4	1	4	1	Lv	6	6	3	1	5	4	
PbS	4	3	1	4	4	4	3	6	3	5	2	4	1	Lv	5	6	3	1	5	4	
Photovoltaic devices																					
Selenium	3	1	6	6	5	0	5	3	0	3	1	2	—	0	5	6	4	6	5	3	
Silicon	5	4	3	3	4	0	3	3	0	2	3	2	—	0	4	5	2	6	2	1	
Photodiodes, silicon																					
Ordinary *p-n*	4	3	2	2	4	1	1	2	2	2	2	1	1	Lv	2	1	2	4	1	1	
PIN Schottky	2	1	2	2	4	1	1	2	2	2	2	1	1	Lv	1	2	2	4	1	1	
PIN diffused	4	3	2	2	4	1	1	1	2	2	2	1	1	Lv	2	2	2	4	1	1	
Phototransistors																					
Silicon	4	3	2	3	2	2	1	2	3	3	2	4	1	Lv	4	1	2	6	2	2	
PhotoFET	4	3	2	2	2	1	1	2	2	2	2	4	1	Lv	4	1	2	6	3	2	
LASCR	4	3	2	5	5	2	2	3	4	2	2	4	1	Lv	4	4	2	6	3	4	
MOS photodiode	4	3	2	2	2	2	2	3	2	2	2	3	1	Lv	3	2	2	4	2	2	
Photomultiplier tube	1	2	1	1	1	1	6	6	5	5	5	1	2	Hv[a]	1	7	4	6	3	5	

[a] Lv = low voltage; Hv = high voltage.

the solid state devices. Linearity of response over the entire dynamic range is essential to good performance. Photomultiplier tubes of comparable cost do not have such linearity. Stability and fatigue effects were of significant interest to the projects success so as to induce the purchase and use of a silicon photodiode (diffused junction) for this project.

Other considerations included in the decision were size requirements, cost, and power supply requirements. In each of these areas, the solid-state device was better suited to the task.

Having decided on the detector, it was necessary to design suitable processing electronics. The photodiode may be operated

in one of two modes:

(1) Photoconductive: The photodiode is biased by a reference voltage

(2) Photovoltaic: The diode is used as a current source and input to an amplifier.

The light levels were anticipated to be extremely low and this then demanded that the detector be used photovoltaically because of the absence of leakage currents. Both systems are illustrated in Figure 19.

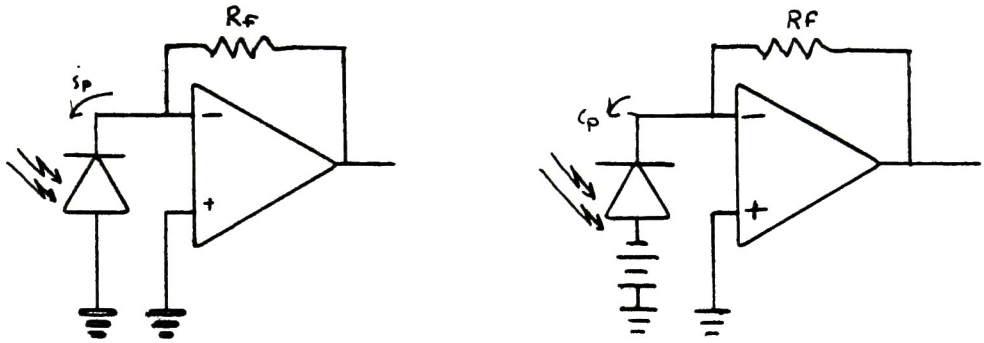

Figure 19 Photoconductive and Photovoltaic Systems

In both cases, the diode is connected to the inverting side of an operational amplifier. The junction of the photodiode and feedback resistor R_f is termed a summing junction and is connected to the inverting side of the op-amp. Because of the feedback, the inverting terminal (labeled (-)) is driven to the potential of the non-inverting terminal. If the non-inverting terminal is at ground, then it may be assumed that the potential between the summing junction and ground will be zero and this terminal may be considered a "virtual" ground.

It should be noted that there is no common current path between the virtual ground and real ground, there only exists a zero voltage potential between the two.

The curative property of feedback in an operational amplifier (in the inverting mode) is to produce the necessary current output to match the current at the noninverting input. By inserting a resistance in the feedback network, a voltage proportional to the input current is generated. This is governed by Ohm's law and is given by

$$V_{out} = i_p \times R_f$$

One can imagine that certain active (voltage/current dependent) devices might be inserted into the feedback loop of an operational amplifier to yield results other than those governed by Ohm's law. For instance, a transistor, when properly biased, exhibits logarithmic V/I characteristics. Proper choice of device will determine the scale of the log, but there exist a number of devices produced solely for this purpose.

For the purposes of this project, eleven circuit variations were tried, of these, two were workable (at the required signal magnitudes) and one was chosen to be the final circuit. Both will be considered in the following discussions.

The first is based upon taking a log of voltage and is diagrammed in Figure 20.

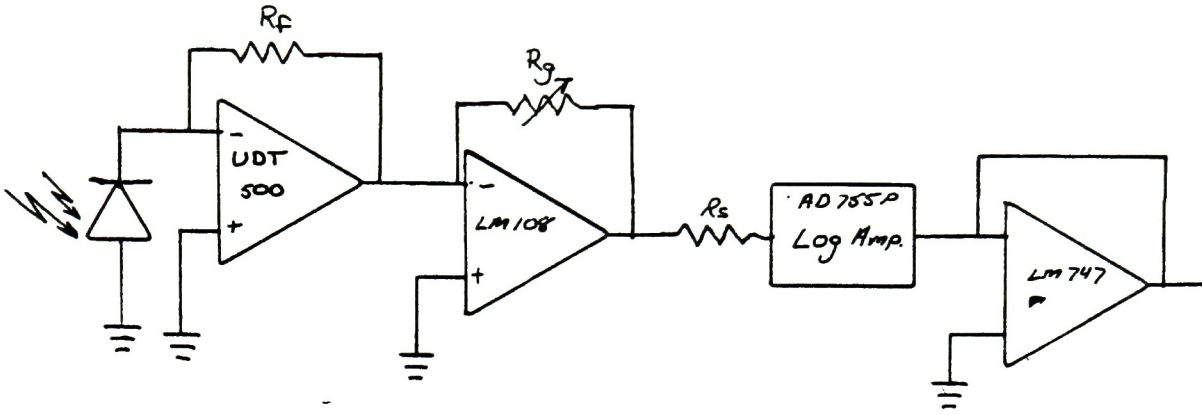

Figure 20 Log of Voltage Configuration

The UDT device is a monolithic photodiode/op-amp which has provisions for setting gain. The next amplifier was used to invert the voltage to minus polarity and adjust level of voltage into the log amp, so as to produce a suitable voltage at the output.

The Resistor, R_s, sets the zero crossing of the log device. The final amplifier is used as a buffer to decrease the output impedance and invert the voltage back to positive for proper measurement.

It was hoped that using a monolithic first stage, stray signal pick-up would be minimized and lower signal levels might be recorded. Logging of voltages, however, limits the dynamic measurement range of the device at the low end of the signal range. This is due to what is termed "offset voltage". This arises from the following considerations:

(1) All amplifiers exhibit an offset current, I_{os}, which is a current that appears at the output when there is no input current at either terminal. Most amplifiers have "trim" provisions to trim the offset to zero. When the offset current is fed through a feedback network, a voltage is developed at the output of the amplifier.

(2) In log amplifiers a reference current is generated for purposes of mathematical continuity, the log is a unitless operator. Hence, what the log amp actually does is take a log ratio such that

$$V_{out} = -K \log \frac{V_{in} - E_{os}}{V_{ref}}$$

when the log of voltage is taken, the resistor R_s, is used to set the reference voltage such that

$V_{ref} = i_{ref} \times R_s$

$E_{os} = i_{os} \times R_s$

$V_{in} = i_{in} \times R_s$

K = scale factor volts/decade

Note that in setting R_s, the designer not only sets the scale and magnitude of the reference voltage, but that of the input and offset currents as well. For the amplifier chosen, I_{os} is internally set to approximately $\pm$ 10pA. When logging currents from 1nA - 1mA this is not such a significant source of error, but when limiting I_{in} by R_s, E_{os} becomes a dependent variable along with I_{in}. This is a systematic, but trimable, error. When logging current, the maximum error due to offset is given by

$$\frac{\pm 10 \text{ pA}}{i_{ref}}$$

For a 1nA input, E = 1.0%.

The voltage input is limited at the low end by other factors such as the V/I current characteristics of the feedback elements and their respective junction characteristics.

It was found in experimentation that the offset trim requirements on all of the active components, became an exceedingly difficult operation and was judged by the designer to be impractical under operational conditions. A review of Figure 20 will show the problem. It is of paramount importance to trim to the UDT - 500 photodiode/amp combination because any offset voltages are magnified by the second stage level shifter such that

$$V_{LSout} = G(ip \times R_f + V_{OSP}) + V_{OSL}$$

where G = gain of the amplifier second stage

ip = photocurrent

R_f = feedback resistance of first stage

V_{OSP} = offset voltage of stage one

V_{OSL} = offset voltage of stage two

Results can get quickly distorted when the log of V_{LS} is taken

$$V_{out} = -K \log \frac{V_{LS} - V_{OS}}{V_{ref}}$$

$$= -K \log \frac{G((ipR_f) + V_{OSP}) + V_{OSL} - V_{OS}}{V_{ref}}$$

Because all of the offset voltages are of similar magnitude the most significant factor is seen to be $G \times V_{OSP}$. Because of the offset requirements the anticipated stability was not attained. The final circuit chosen, though still not optimal, represented the best compromise of design considerations.

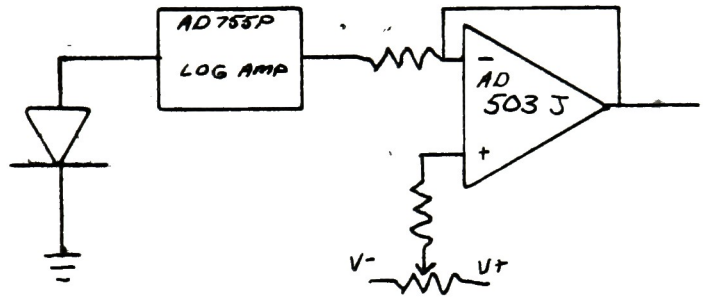

Figure 21 Final Configuration: Log Current

The first stage is a 10DB/541 photodiode, acting as a current source. This is D.C. coupled to the log amplifier which is inturn fed into a F.E.T. inverting operational amplifier. The resultant transfer equiation is

$$V_{out} = V_{set} - K\log\left(\frac{ip - ios}{i_{ref}}\right)$$

V_{set} is a voltage used to set zero.. As the signal changes with negative unity gain, the inverting amplifier acts as a differencing amp and the resultant voltage is a result of the difference between the log amp output and V_{set}.

The inverting amplifier used was an Analog Devices 503J, F.E.T. input opamp. It possess low offset characteristics (< 50 mV absolute max), but when used in a differencing mode, this is not needed. It's major advantage is its high input impedance and stability.

As stated earlier, the offset current of the AD-755P log amp was suitable to allow a maximum of 1% error when referred to input current over its required ranges. This means that there are no offset adjustments to be made.

The final board configuration is pictured in Figure 22.

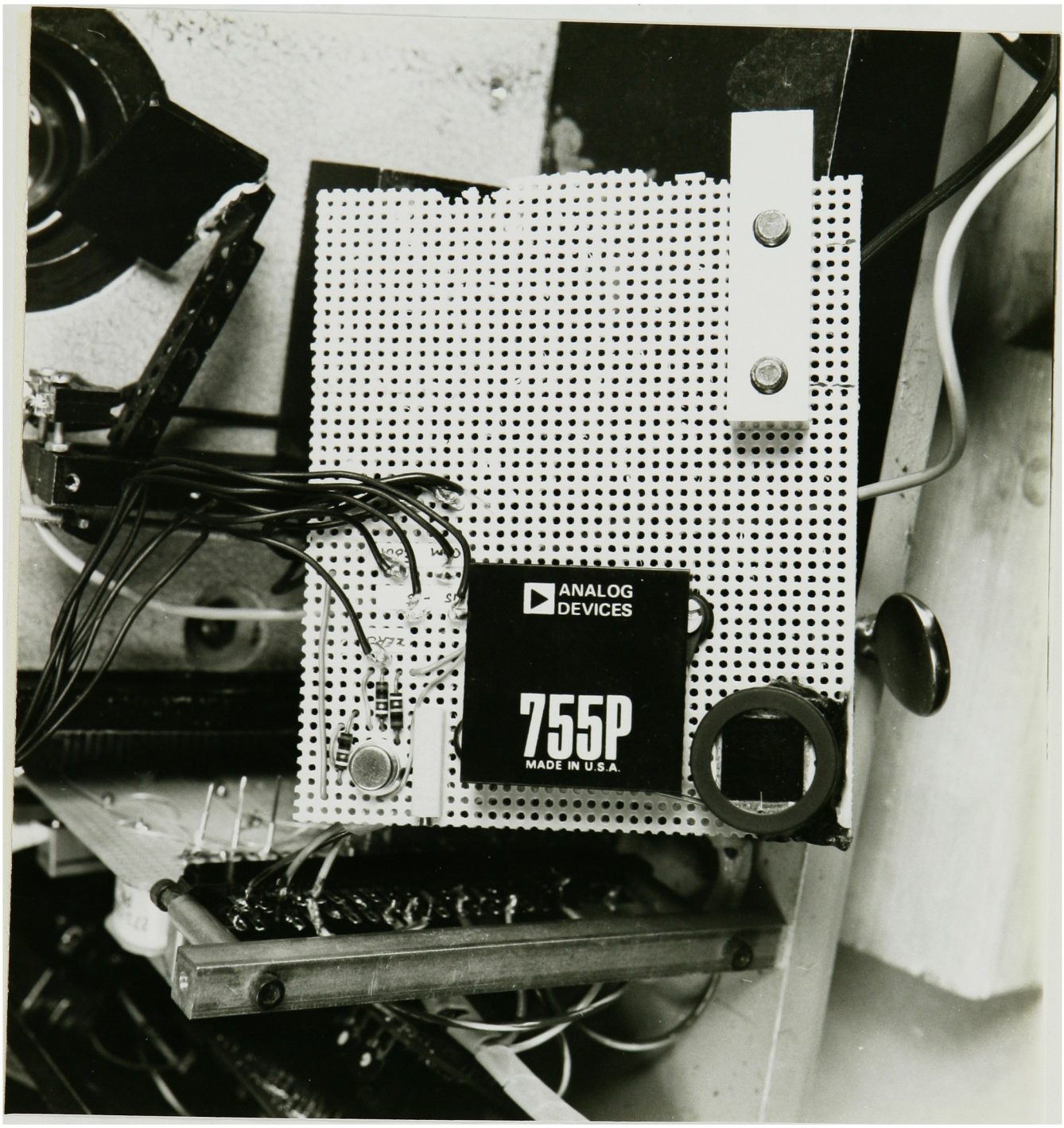

Figure 22 Photograph of Radiometric Board

3.4 The Optics

The optical system is comprised of four subsystems: the aperture illumination system, the influx system, the efflux system, and the focus illumination system. It will be seen that the influx and efflux systems serve a dual role in the operation of the system. A diagram is given in Figure 23.

The aperture illumination system (Figure 24, lower half) is used to provide illumination for the scanning apertures. It is comprised of five main components: a spherical reflector, a lamp, a cold mirror, a biconvex lens, and a sharp cut-off spectral filter (low pass). The reflector (1) forms a 1:1 image of the filament of the lamp (2). The radiation below 800nm is reflected by the cold mirror (3) and the condenser (4) is set to focus an image of the filament into the entrance pupil of the influx system. The short pass filter(5) is used to further limit the longest wavelength passed to 680nm.

The influx system (Figure 24, upper half) is comprised of three main components: the aperture plate, eyepiece assembly, and the objective. The aperture (6) is imaged using the eyepiece/objective combination (7&8) onto the film. In normal scanning operation the moving reflector (9) and second eyepiece (10) are not used. These components are focus aids and will be described later on.

The apertures were produced photomechanically in brass. Art work was prepared at a magnification of 4x and reduced to a negative and contacted onto the brass covered with Kodak KMER resist. The apertures are normally behind a screen which allows only one to be

1. sperical reflector
2. lamp
3. cold mirror
4. condenser lens
5. band pass filter
6. aperture wheel
7. imaging eyepiece
8. objective
9. viewing mirror
10. viewing eyepiece
11. sample stage
12. collection/viewing condenser
13. detector
14. moving mirror for focus illumination
15. focus illumination condenser
16. focus lamp

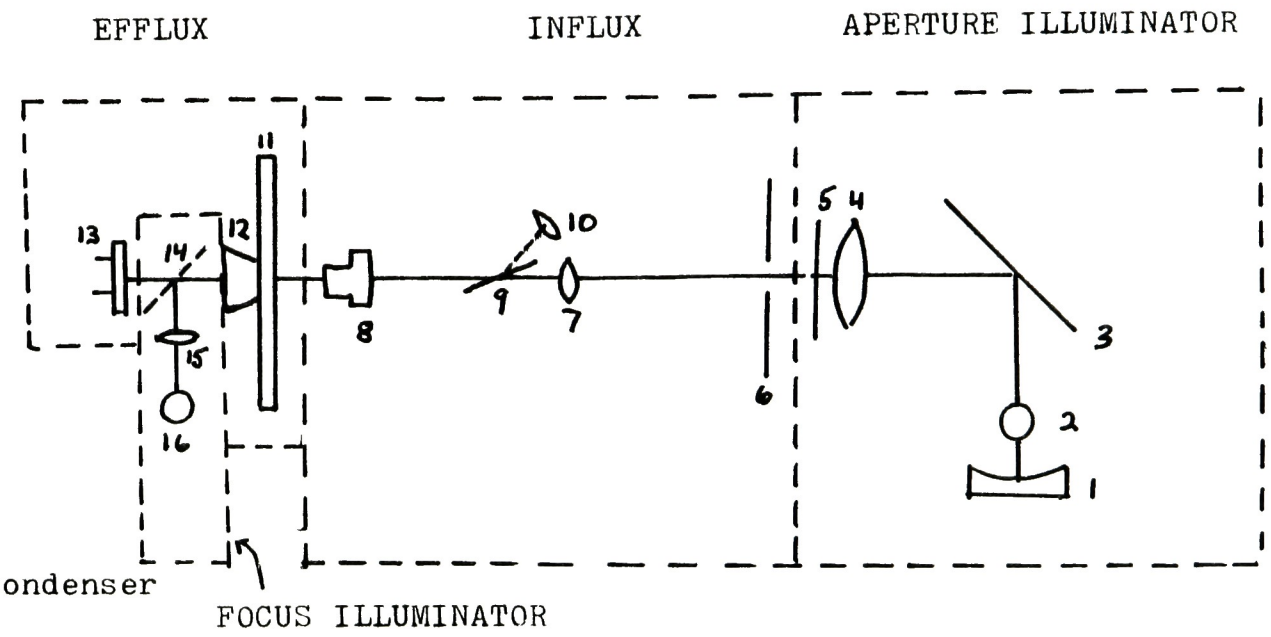

Figure 23. Optical system component diagram

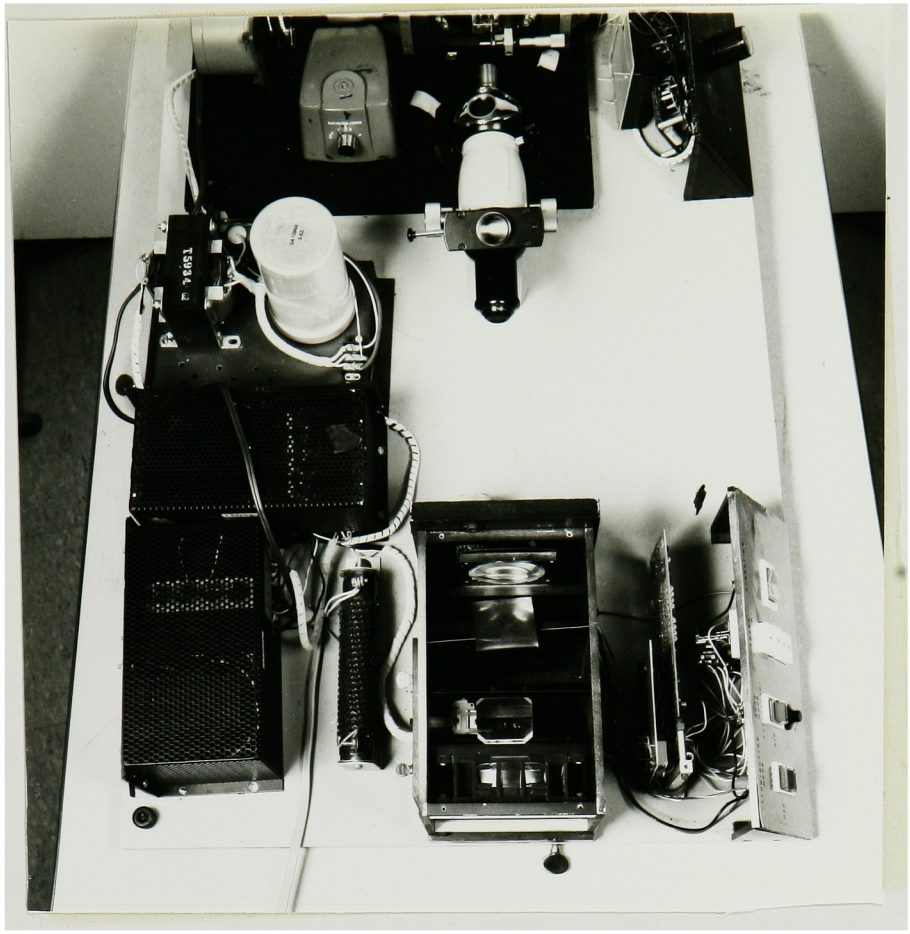

Figure 24. Influx optical system

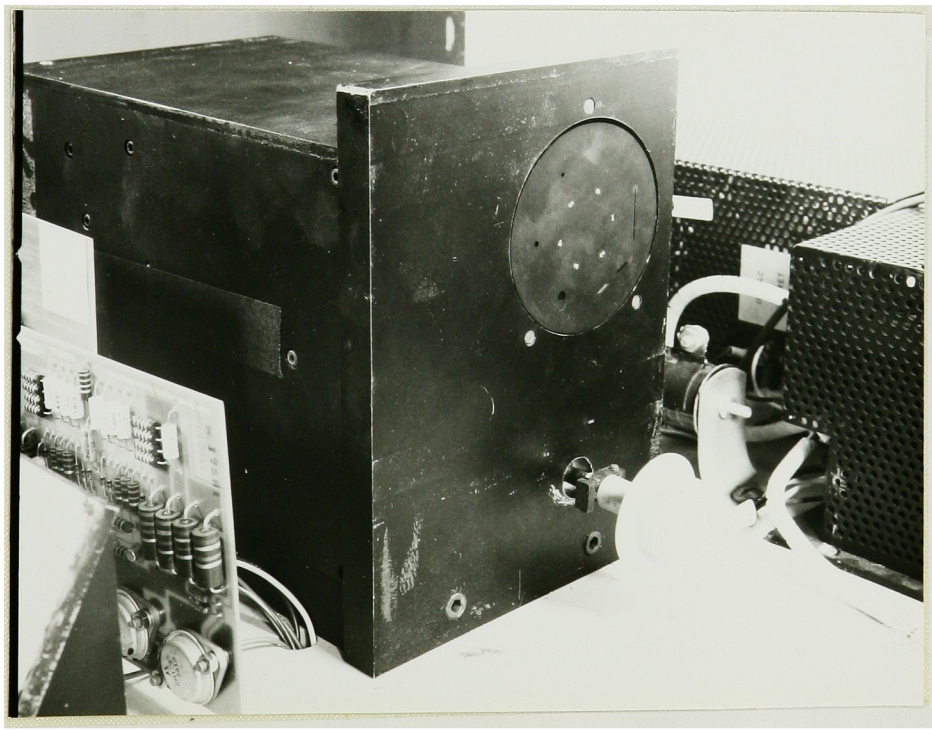

Figure 25. View of Aperture Wheel

projected at a time. Figure 25 is a photograph of the apertures which may be rotated into place using the knob near the base of the illumination subsystem. Aperture sizes are given in Table 2.

Aperture Number	Size
1	0.425 x 20 mm
2	1.546 x 20 mm
3	2.873 mm
4	2.153 mm
5	1.511 mm
6	0.426 mm

Table 2 Aperture Sizes

Each aperture was measured on a Nikon measuring microscope five times and a mean value is given in the above table.

The efflux system has three components: the stage (11), the condenser (12) and detector (13). The condenser is a standard, high umerical aperture microscope condenser, but it is not liquid gated to the stage. This limits the N.A. to a value less than or equal to 1.0. The film is not focused onto the detector, but in a region somewhat before the detector. The only constraint is that the photodiode be underfilled under all conditions of measurement. This is a power, rather than irradiance, measurement is required by the mathematics. Figure 26, is a "diode's-eye-view" of the efflux system.

The final sub-assembly is the focus illuminator and it is comprised of three components and it shares the high numerical aperture condenser with the efflux system.

System focus is accomplished in one of two manners. When the "illumination" switch on the front panel is thrown to "focus" a

solenoid is activated and this moves the focus illumination mirror into place (see Figure 26). When this mirror is in the correct position, a micro-switch activates the focus illumination system (15,16). The condenser acts as an illuminator instead of a collection lens. An enlarged image of the film is projected back onto the aperture plate. When theimage of the film is in focus on the aperture plate, one may safely assume that an image of the aperture plate will also be in focus on thefilm. (They are conjugate planes.) If a sample is of sufficient density as to prevent examination of the image on the aperture, the moving reflector (9) and supplementary eyepiece (10) may be alternately used to aid in the focus (after the supplementary eyepiece has been set par-focal with the best aperture plane focus at low magnification!).

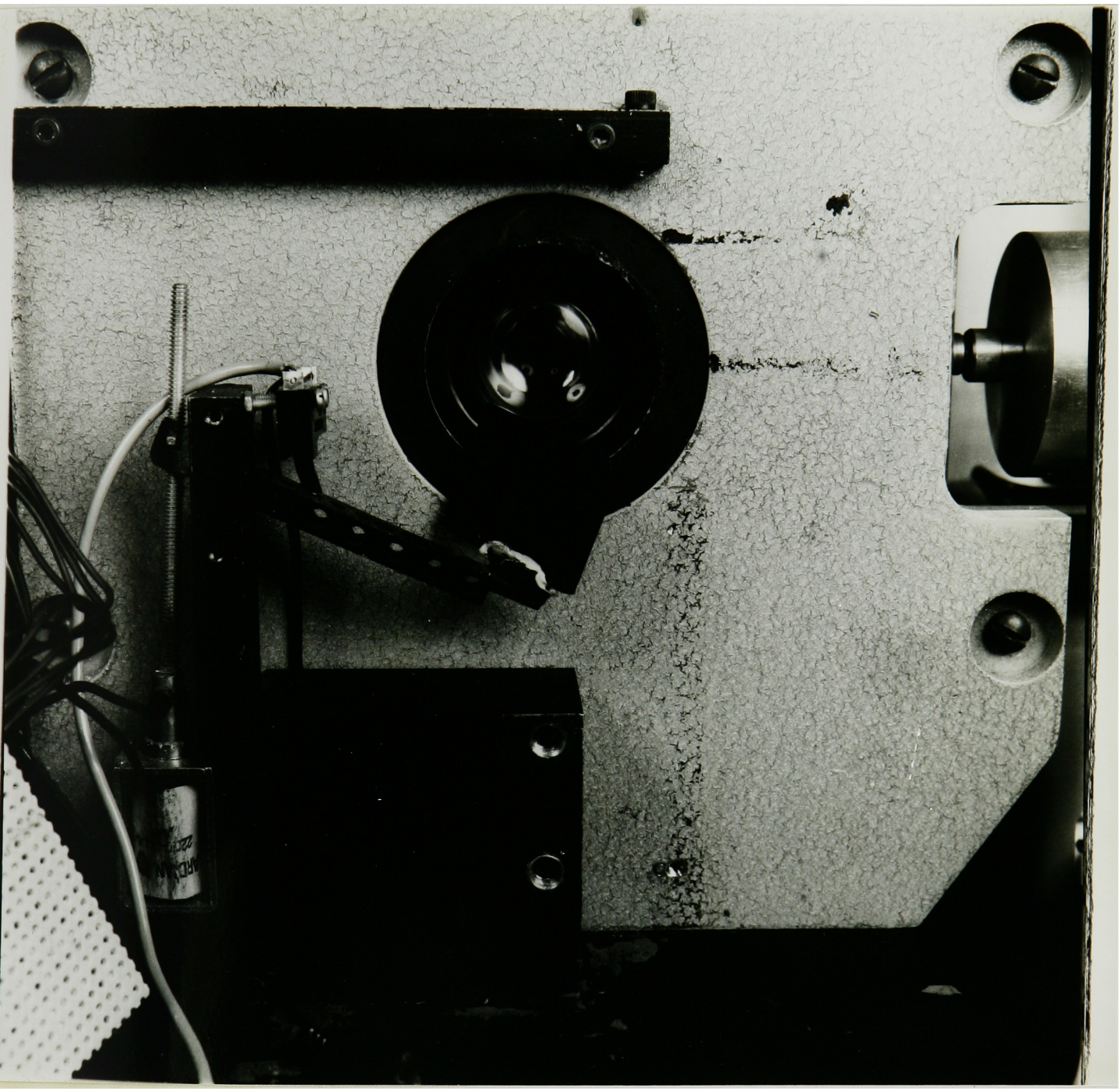

Figure 26. Photodiode View of the Collection System

4 Results

Testing a microdensitometer's performance is a three-fold problem: the optical response, photometric response and spatial integrity.

Because of the slight translation of the stage with each step, it would be necessary to measure stage motion with some form of interferometer. This equipment was not available at the completion of this work and no measurement of spatial integrity could be made. An estimate of error can be made if the manufactures specifications can be believed.

The stepping motor used was guaranteed to have a stepping angle error no greater than 5% per step. This corresponds to angular error per step of 0.045° or 2.5' arc of the lead screw. Assuming a perfect micrometer screw of 500 μm/revolution, the spatial error due to the stepping motor is 0.1606 μm. Nonuniformities in the lead screw are not known but high quality micrometer threads are generally good to .005"/inch or 5 μm/mm cumulative error. If we assume that 1 μm of motion is independent of the next μm of motion, and that there are 1000 such motions whose total expected variance is 5 μm, the variance per step may be estimated to be s^2 = .0707 μm/step. Assuming that the 5% specification of the stepping motor is a one standard deviation limit, the total variance per step may be estimated to be .0965 and the standard deviation would be around .3 μm. The sample spacing may then be estimated to be 1.25 μm $\pm$ .6 μm, 96% of the samples taken. This may be considered a somewhat pessimistic figure.

To test the photometric response of the instrument Schott glass filters were inserted into the light path to modulate the beam. The

test was run five times at each aperture setting and linear regression was performed on each data set. The regression was performed over two ranges of density 0 - 3.88 and 0 - 2.68. The machine was zeroed to D = 1.15 with the 1.15 Schott glass filter in place. The results are tabulated in Table 3.

	Aperture	Slope	Intercept	r^2	r
Range 0-3.88	1	.956	.059	.9994	.9997
	2	.935	.088	.9995	.9997
	3	.946	.088	.9993	.9996
	4	.951	.084	.9992	.9996
	5	.957	.060	.9993	.9996
	6	Results not applicable, see *			
Range 0-2.68	1	.987	.0147	.9994	.9997
	2	.965	.041	.9997	.9998
	3	.978	.041	.9993	.9996
	4	.9907	.026	.9996	.9998
	5	.9923	.0097	.9996	.9998
	6	.993	.005	.9999	.9999

* Aperture 6 is not designed to be used at density >3.

It should be noted that there is an increase in performance as the apertures get smaller. Aperture 6 is the 1.3 μm spot aperture. It was found that it measured the higher densities (but below 3.0) more accurately than the other apertures. This is primarily due to flare in the optical system in the large apertures. Aperture 2 is the largest aperture and it is noted that the slope is lower and the intercept is higher in both cases than any of the other apertures. This is because the higher densities have been suppressed by the optical system flare.

The next test was to actually scan a step tablet. An EIKONIX microdensitometer Q.C. target was scanned and compared to diffuse density values measured on a MacBeth TD 102 Densitometer. These are displayed in Table 4. The machine was zeroed on a clear area of film Aperture 6 was used for the test.

Diffuse Density	Microdensity	Standard Deviation
.05	.060	.007
.12	.118	.011
.52	.51	.0071
.89	.928	.019
1.38	1.481	.0143
2.23	2.418	.025

It is noted that there tends to be a trend to increase density at the high end of the scale. The immediate reaction to such a trend is to assume that the instrument is no longer a total collection system. This may or may not be the case due to the fact that density at the true micro level is zero or infinite. This may account for the increase in density as well. The output did not drift more than .01 density units in 12 hours of operation. This is due to the solid state electronics and the sample scanning configuration which allows for wide variations in focus with little or no variation in photometric zero.

One of the most crucial aspects of microdensitometer performance is its optical quality. The most interesting feature of a "linear" microdensitometer is that the machine's modulation transfer function is simply the Fourier transform of the image of the sampling aperture. The image of the sampling aperture may be thought of as the reduced influx aperture convolved with the influx lens point spread function*. In Fourier space this becomes the Fourier transform of the reduced aperture multiplied by the transfer function of the optical system. In testing this microdensitometer, the slit apertures were not employed for two reasons: they exhibited the highest flare effects and they were prone to misalignment problems.

Figure 27 is a plot of the polychromatic transfer function of the 25x lens and receiver system along with the modulus of the raw transfer functions of a 1.3, 4.8, 6.8 and 9.1 μm spot apertures. The multiplication of these functions was performed and a predicted transfer function was calculated for each aperture. Measurements were then made using an NBS edge. The results of the edge trace were converted to transmission, the derivative taken and then Fourier transformed. These are plotted in Figures 28, 29, 30, and 31. The plotted transfer functions represent the best of four independent tests of each aperture and should only be used as indicators of operational performance rather than limiting values. It should be noted that the 1.3 μm and 6.8 μm apertures differ considerably from the predicted performance. In the case of the 1.3 μm aperture it may be assumed that the MTF of the lens is the limiting function. This is illustrated in Figure 31. It is

* While the condition of linearity is independent of coherence conditions in a totally collecting system, the transfer function of the influx objective is most definately not independent of coherence effects! The degree of coherence of the source in the exit pupil of the influx objective plays a profound role in the ultimate transfer function of the final instrument.

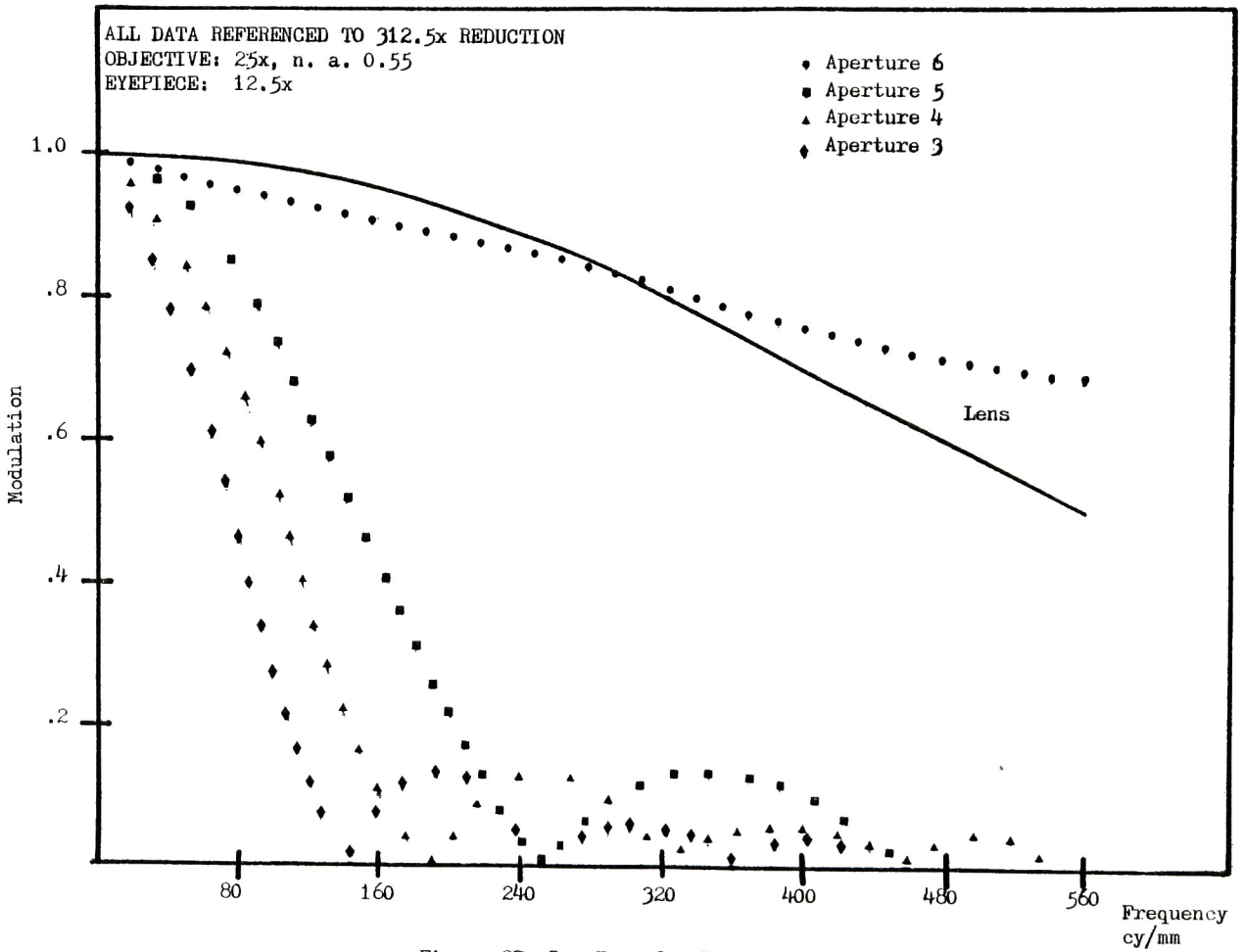

Figure 27 Raw Transfer Functions

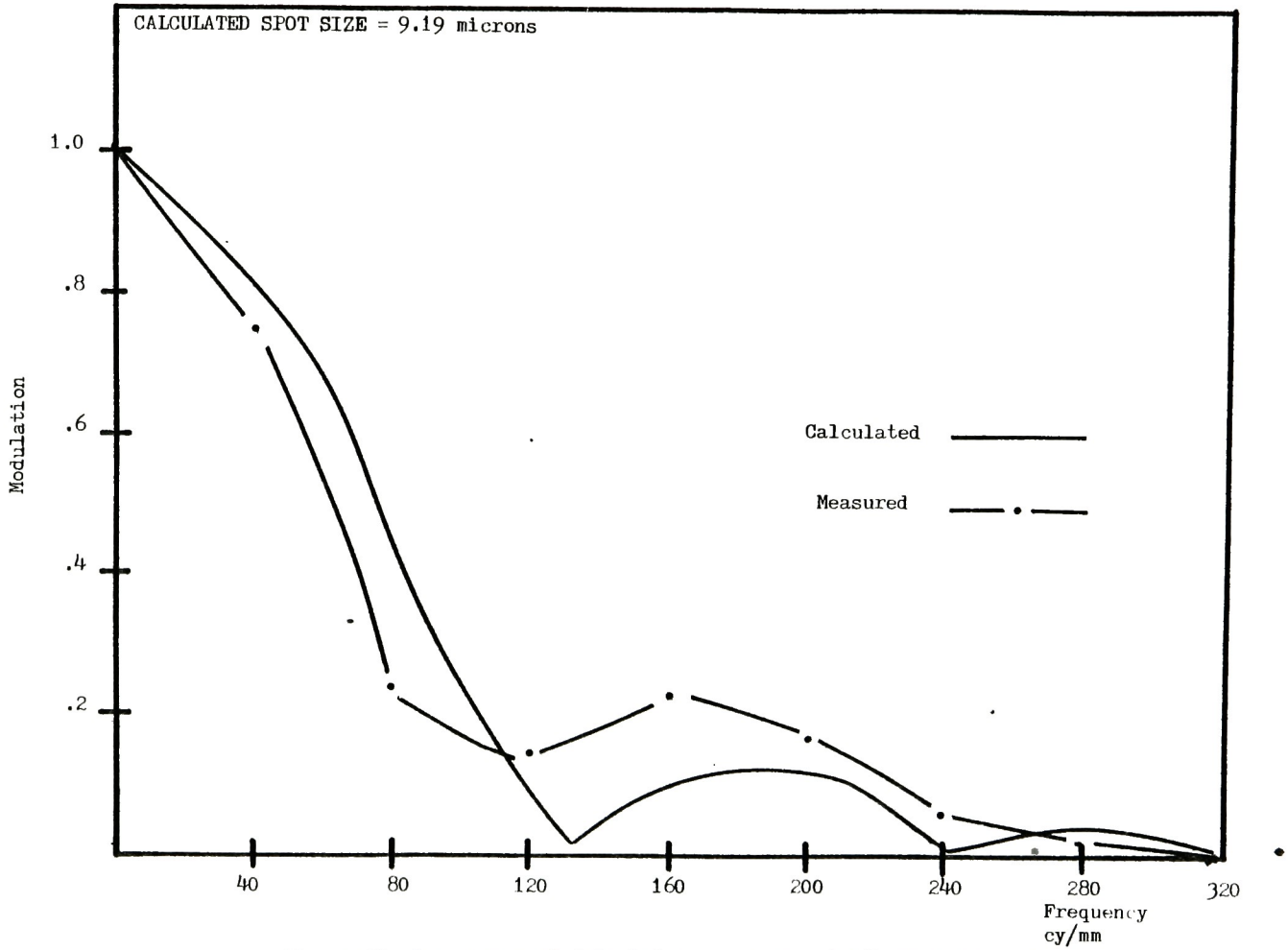

Figure 28 Comparison of Calculated and Measured MTF of Aperture 3

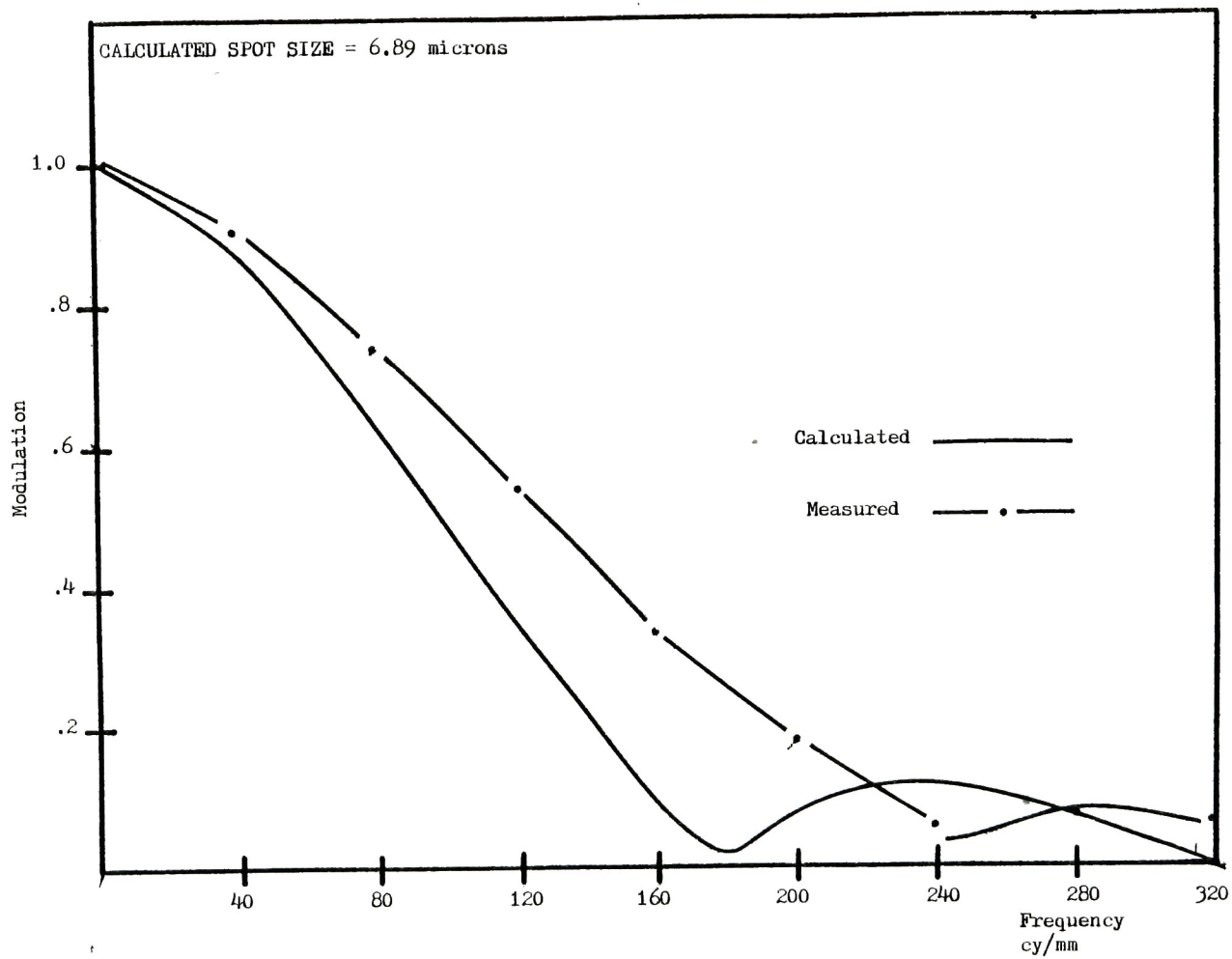

Figure 29 Comparison of Calculated and Measured MTF for Aperture 4

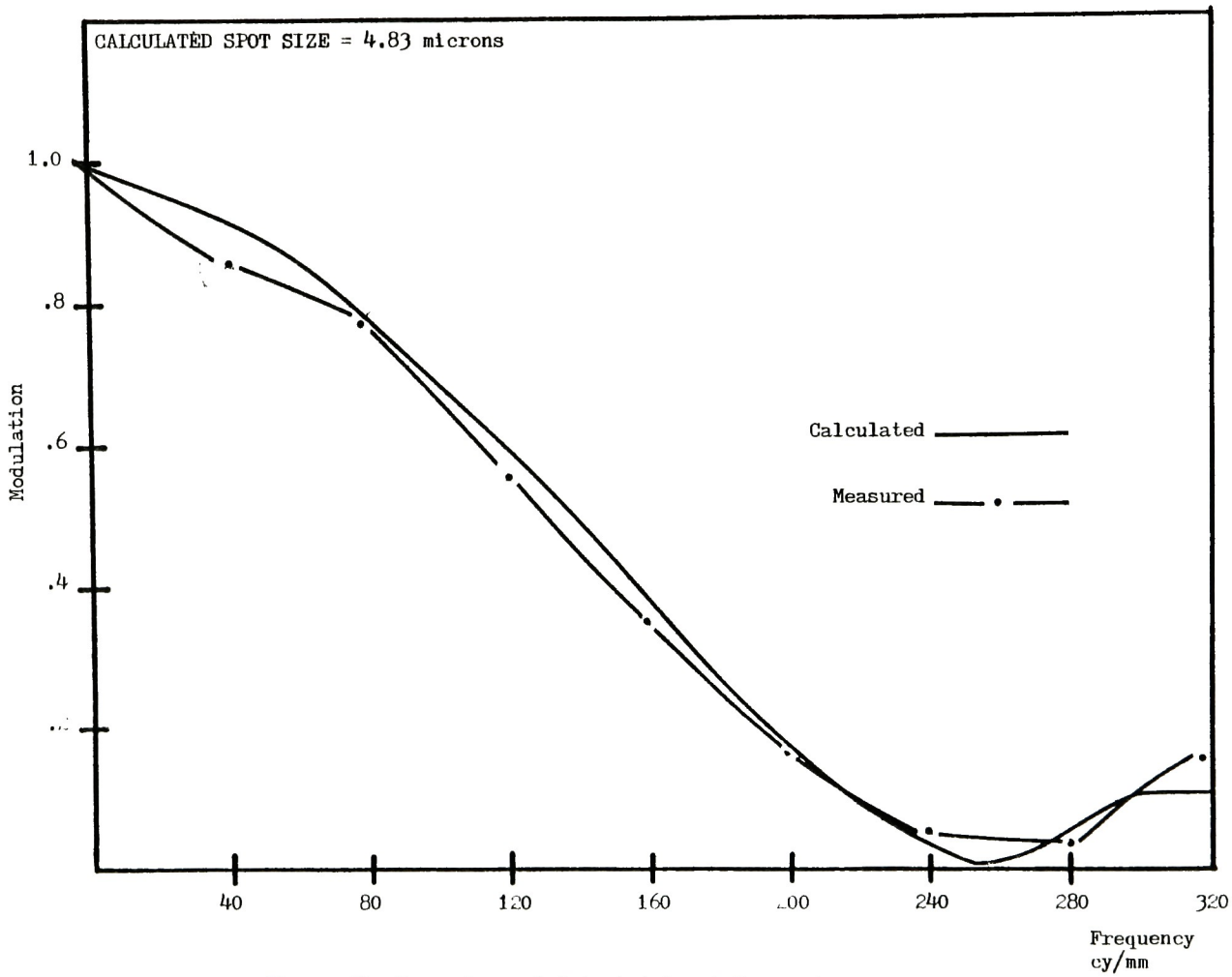

Figure 30 Comparison of Calculated and Measured MTF for Aperture 5

Missing Page

seen that the aperture transfer function is actually higher than the lens transfer function. It must be noted that the eyepiece in the reduction microscope has been left out of the analysis and it may be possible that the transfer function of this element plays a significant role with objects of small extent in the aperture (object) plane. The focus of the instrument is really quite critical and it is possible that the tolerances are such that the instrument can not be focused reliably at the smaller aperture.

The 6.8 μm aperture is another case. In this test, the results were higher than predicted. This is cause for concern, because it may indicate a nonlinearity in response. There is no rational explanation why this aperture should perform better than predictions, other than a change in coherence of the source or a sampling problem. It is not known what change occured.

5 Conclusions and Recommendations

The work done here has demonstrated the potential of the "linear" design. In general, the design offers a much higher level of radiometric integrity when used with small apertures. It is plagued by flare and must be used in a darkened environment to be useful. This comes as a direct consequence of its collection system. Short of wetting the condenser to the stage and the sample to the stage, little can be done to improve the collection efficiency of the condenser.

There are still a great many questions to answered about the coherence properties of the instrument. Because of the nature of the system the transfer function is very dependent upon coherence at the aperture plane. It should be possible to selectively enhance certain bands in the transfer function of the instrument by adjusting the coherence of the source. Substitution of a laser should yield a flat transfer function out to one half the diffraction limited cutoff of the objective, with no change in the linearity of the instrument. This is assuming a total collection system.

The specific recommendations that the author wishes to make are the following:

(1) The instrument should be rewired. All power supplies and control electronics with the exception of the log amplifier board should be located off of the main instrument in suitable enclosures.

(2) Substitution of the current log amplifier AD-755P with an Intech Function Modules Model - 531 log Amp could extend the low end dynamic range of the instrument by two decades.

(3) The stage sample holder should be reworked to allow for easier sample mounting.

(4) The illumination system should be redesigned to allow for projection onto a white screen on the aperture plane for ease in focusing.

The total cost for such a modification should be under $300.00 (excluding labor).

As it stands, the instrument should <u>not</u> be used because of the nature of the wiring. It is inherently unsafe.

The optics of the instrument and the electronics have proven themselves in terms of performance. Further development should be carried out to make the instrument useable by the majority of students.

BIBLIOGRAPHY

1. D.N. Grimes, J. Opt. Soc. Am., 61, 1263 (1971)

2. R.E. Swing, J. Opt. Soc. Am., 62, 199 (1972)

3. R.E. Kinzly, J. Opt. Soc. Am., 62, 386 (1973)

4. D.J. Cronin and G.O. Reynolds, Opt. Eng., 12

5. R.E. Swing, PROBLEMS OF LINEAR MICRODENSITOMETRY, 16 May 1975, Final Report on Contrac t No. F33615-71-m5007 for Air Force Avionics Laboratory, Wright-Patterson Air Force Base, Ohio

6. Technical Operations Incorporated, DESIGN STUDY FOR A NEW GENERATION MICRODENSITOMETER, March 1973, Final Report on Contract F30602-72-C-0322 for Rome Air Development Center, Griffis Air Force Base, New York

7. A. Stimson, Photometry and Radiometry for Engineers, (John Wiley and Sons, New York, 1974) p. 20

8. Superior Electric Catalog MD1741

APPENDIX 1

Derivation of the Paraxial Mutual Intensity Function Propagator used in the Theory Section of this Thesis

$$\Gamma_{1,2} = \psi_{object}(\alpha_1)\,\psi^*_{object}(\alpha_2) \qquad \text{(A-1)}$$

The notation used in this thesis is very compact. This situation arises because the equations and resultant integrals contain many variables and classical notation would become quite cumbersome. When describing the mutual intensity function as a time average and spatial correlation as in A-1, a number of points should be noted:

(1) The arguments α_1 and α_2 are really representative of a position given by two coordinate points (cartesian or polar) in a plane.

(2) As a result of (1) each one-dimensional integral is, in fact, a two-dimensional integral.

(3) To fully characterize the field after it has been propagated, requires that Γ_{12} be generalized to some function $\Gamma_{n1,n2}$ and all points in the field be considered. This is not realistically feasible and the field is assumed to be stationary. This implies that it is the absolute <u>difference</u> between two points in a field rather than their absolute <u>position</u> which determines the nature of $\Gamma(\alpha_1, \alpha_2)$.

The Zernicke Formula for the propagation of the mutual intensity function is given by A-2,

$$\Gamma(q_1 q_2) = \Gamma(p_1 p_2)\,\frac{e^{ik(z_1-z_2)}}{z_1 z_2}\,\Lambda_1\,\Lambda_2^* dp_1 dp_2 \qquad \text{(A-2)}$$

The coordinate system for the above equation is given in Figure A-1.

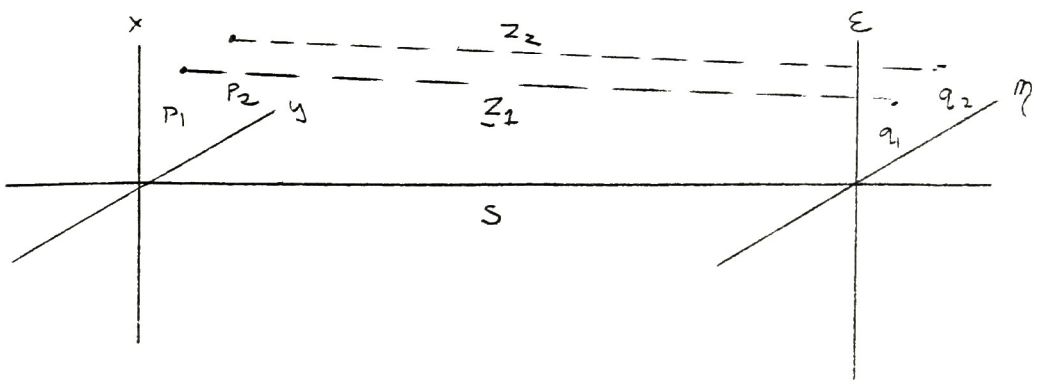

S is the orthogonal distance between the two parallel planes of interest. Z_1 is the distance from p_1 to q_1 and z_2 is the distance from p_2 to q_2. The cartesian coordinates x,y describe p_1, p_2 and ϵ, η describe the location of q_1 and q_2. Λ_1 and Λ_2 are inclination factors which shall be considered constant in the paraxial region. If we let p_1 be represented by $(x_1 y_1)$ and q_1 be represented by (ϵ_1, η_1) the length z_1 may be shown to equal the expression in A-3 (by Pythagorem's theorem):

$$z_1^2 = (x_1 - \epsilon_1)^2 + (y_1 - \eta_1)^2 + s^2 \qquad \text{(A-3)}$$

This calculation shall be depicted as in A-4 and A-5.

$$z_n^2 = ((p_n - q_n)^2 + s^2) \qquad \text{(A-4)}$$

where $(p_n - q_n)^2 = (x - \epsilon)^2 + (y - \eta)^2$.

$$z_n = ((p_n - q_n)^2 + s^2)^{\frac{1}{2}} \quad . \qquad \text{(A-5)}$$

In equation A-2 the term $z_1 z_2$ in the denominator is seen to affect only the amplitude of the results. For the paraxial region this is essentially constant and it (along with the inclination factor) is now brought outside of the integral as a constant. The term is left in the exponent because it determines the phase which may be be assumed to be constant.

$$(q_1 q_2) = k \int \Gamma(p_1 p_2)\, e^{ik(z_1 - z_2)}\, dp_1 dp_2 \qquad \text{(A-6)}$$

Referring to equation A-5 one may factor out s^2 to yield

$$z_n = \left(s^2\left(\frac{(p_n - q_n)^2}{s^2} + 1\right)\right)^{\frac{1}{2}}. \qquad \text{(A-7)}$$

If one lets $\frac{(p_n - q_n)^2}{s^2} = x$ it is noted that the expression under the second set of parenthesis is of the form $(x+1)^{\frac{1}{2}}$. A simplification may be made by making use of the binomial series for this function (A-8) and

assuming that $s_n^2 \quad (p_n - q_n)^2$. (i.e., the terms higher than the second may be neglected, as in A-9.)

$$(1 + x)^{\frac{1}{2}} = 1 + \frac{x}{2} - \frac{1}{2 \cdot 4} x^2 + \frac{1 \cdot 3}{2 \cdot 4 \cdot 6} x^3 \ . \ . \ . \tag{A-8}$$

$$z_n \doteq s\left(1 + \frac{(p_k - q_k)^2}{2\, s^2}\right) \tag{A-9}$$

and

$$z_n \doteq s + \frac{(p_k - q_k)^2}{2s} \quad . \tag{A-10}$$

Substitution of A-10 into A-6 yields

$$\Gamma(q_1 q_2) = k \int \Gamma(p_1 p_2) e^{ik\left(s + \frac{(p_1 - q_1)^2}{2s}\right)} \quad e^{-ik\left(s + \frac{(p_2 - q_2)^2}{2s}\right)} \quad dp_1 dp_2 \tag{A-11}$$

the term $e^{iks} \quad e^{-iks}$ are constant and are brought out of the integral to yield

$$\Gamma(q_1 q_2) = c \int \Gamma(p_1 p_2)\ e^{\frac{ik(p_1 - q_1)^2}{2s}} \quad e^{\frac{-ik(p_2 - q_2)^2}{2s}} \quad dp_1 dp_2 \tag{A-12}$$

Please note that the form of the propagator is exactly that of the one used in Section 2.3.

APPENDIX 2

Phase Term Introduced by a Lens in a Plane

The function of a lens, from the standpoint of physical optics, is to convert a plane wave front into a spherical wavefront of radius "f". Here, P is the plane wavefront, L, the perfect lens, and S is the spherical wavefront. We let ρ = the radial height from the axis to a point on the spherical wave.

By the Pythagorean theorem, we have:

(1) $(f - x)^2 + \rho^2 = f^2$

or

(2) $2xf = \rho^2 - x^2$.

For paraxial optics x is small and x^2 is thus negligible and we have:

(3) $x = \frac{\rho^2}{2f}$.

The phase (ϕ) introduced is this:

(4) $\phi = kx = \frac{k\rho^2}{2f}$.

This phase term is introduced into the equations as

(5) $e^{ik\phi} = e^{\frac{ik\rho^2}{2f}}$.

For a partially coherent complex field the function is given by

$$f(\rho_1)F^*(\rho_2)\exp(ik(\rho_2^2 - \rho_1^2)/2f).$$